The authors would like to thank both reviewers for their most constructive and valuable comments. Below, we address the author comments in the order they were received. A marked-up version of the manuscript prepared with Latexdiff is included with this author comment. Additionally, in response to reviewer feedback, we have added a supplementary materials section to the revised manuscript, which is included with this comment as well.

Response to Comment by Reviewer #1

1 General Comments

> This is a nice paper, which I enjoyed reading very much. I recommend it for publication if my criticisms below can be addressed (may need "Major revisions").

Thank you for these encouraging and most helpful comments. We addressed them in the revised manuscript, and fully describe our revisions below.

2 Specific Comments

2.1 Major Comments

- **p2959, L22:** Herman (2010) discusses a stochastic (GLV: Generalised Lotka-Volterra) mechanism for generating a Pareto distribution – did the authors look into this at all?

  We thank the reviewer for this reference. While it was cited in the original submission, we agree that it is very relevant and deserves more discussion in the paper, as does Toyota et al. (2011). We added the following to the end of the introduction section.

  > Herman (2010) modeled the FSD as a generalized Lotka-Volterra system, which admits as a solution a Pareto distribution of floe sizes, and suggested that this distribution might fit observed FSDs. Toyota et al. (2011) showed that observed FSDs in the Weddell Sea may be fit by a power law and, that such a scaling relationship may be obtained by assuming that ice fracture is a self-similar process, following a renormalization group method.

- **p2970–2972:** A limitation of this approach is that it only involves binary collisions. Direct numerical solutions (eg [4, 8]) have shown clear grouping and [4] showed the group size had a power-law distribution. This could be an interesting way to look at this, especially in combination with the thermodynamics part (letting the groups freeze together if it's cold enough).

  Our model indeed considers binary collisions only and we acknowledge this explicitly now. We also note in the revised paper that interactions that form aggregate clusters of floes may be generated as a sequence of binary interactions, which is also the manner in which Herman (2013) developed clusters. We clarify and address this in section 2.2 as follows,

Here, interactions between floes are treated as binary collisions, and our model does not consider multiple simultaneous collisions in a single time step. Such multiple collisions lead to clustering, which is relevant for granular media undergoing deformation (Shen and Sankaran, 2004), with sea ice being a possible example. However, Herman (2013) demonstrated in numerical simulations that floes may also aggregate into clusters via a sequence of binary interactions between pairs of floes.

- p2972 L17: "This choice eliminates the need for keeping track of sea ice morphology". If the model can produce a good estimate of ridging history (even just a ridging density), both [2] and [6] observed that floe break-up mostly happened at pre-existing weaknesses (cracks and ridges), so there could be some way of connecting floe size distribution with ridge density in the case of wave break-up.

Our model indeed does not keep track of ridging history, and that its role in later mechanical interactions is an interesting issue. Although adding such physics is beyond the scope of the present article, we now write at the end of section 2.2,

> Given that our model assumes each floe has a uniform thickness, we treat floes formed by ridging or rafting to be of such uniform thickness, chosen to conserve volume. This choice eliminates the need for keeping track of sea-ice morphology. Observations (Collins et al., 2015; Kohout et al., 2015) have indicated that floes may break up along ridges, in which case equation (18) may be used to provide information about the ridge density. This is a potential future extension of the present work.

- p2974 L15: It is worth discussing/mentioning [7] here.

Thanks for this reference to Meylan et al. (2014), which we now cite in Sec. 2.3 in the context of observations and modelling of wave attenuation in ice.

> Future applications of this FSTD model should therefore carefully consider the wave attenuation formulation, based on both model estimates and observations (e.g., Meylan et al., 2014).

- p2975 L10: here the amplitude depends on $d\lambda$ – is this not a problem?

This seemingly unusual formulation is standard in the surface wave literature, where $d\lambda$ corresponds to the finite sampling resolution that separates Fourier components of a wave record. We now make this more explicit as follows,

> The amplitude of waves with wavelengths in the range λ to $\lambda + d\lambda$ is approximated following $a(\lambda) \approx \sqrt{2S(\lambda)\,d\lambda}$ (see Bouws et al. (1998), p.11, and Meylan et al. (2014), eq. 2). The spectrum $S(\lambda)d\lambda$ is equal to half the mean amplitude squared of waves belonging to waves with wavelengths between λ and $\lambda + d\lambda$, equal to the total wave energy in this wavelength band normalized by ρg. The range $d\lambda$ corresponds to the sampling resolution of Fourier components of the wave record (Bouws et al., 1998).

- p2975 L19 The authors are correct that wave heights are roughly Rayleigh distributed (assuming a Gaussian distribution of wave elevations [1] – ie this doesn't apply to mono-chromatic waves (swell waves)).

We have expanded the discussion to include a mention of this limiting case, in Sec. 2.3 as follows,

> The normalization by $A(\mathbf{r}) = \int P_{wa}(a(\lambda))\theta(\epsilon_{crit}(\lambda, \mathbf{r}) - \epsilon_{max})\theta(r - \lambda)d\lambda$, where $\theta(x)$ is the Heaviside step function, assures that the integral of P_f over all wavelengths is equal to 1 if the floes of size $\mathbf{r}$ will break. ... In the case of monochromatic swell waves, which are not described by a Rayleigh distribution, the only contribution of $P_{wa}(a(\lambda))$ to $P_f(\mathbf{r}, \lambda)$ is at the wavelength of the swell, as the wave amplitude $a(\lambda)$ is zero for all other wavelengths.

However, I am not sure that it is correct to apply it to individual wave frequencies or frequency bands. Williams et al. (2013a) used a Rayleigh distribution for the strain spectrum, so the breaking probability considering the full spectrum was proposed to be:

$$P_{breaking} = \mathcal{P}(|\epsilon| > \epsilon_{breaking}) = \frac{2}{\bar{\epsilon}^2}e^{-\frac{\epsilon_{breaking}^2}{2\bar{\epsilon}^2}}$$

This could be used as the total breaking probability but it doesn't give any idea about the floe sizes produced by the breaking. The authors are suggesting using the wave spectrum to get the floe sizes, which is not a bad idea. It could be used in conjunction with the above perhaps, eg.

$$P_f(\mathbf{r}, \lambda) = P_{breaking}\theta(r - \lambda/2)\frac{\int\limits_{\lambda}^{\lambda+\Delta\lambda} S(\lambda')\,d\lambda'}{\int\limits_{0}^{2r} S(\lambda')\,d\lambda'}$$

$$P_{breaking} = \int\limits_{0}^{\infty} P_f(\mathbf{r}, \lambda)\,d\lambda = \int\limits_{0}^{2r} P_f(\mathbf{r}, \lambda')\,d\lambda'.$$

The reviewer's suggestion is a good one, as it addresses the problem of determining the fraction of the ocean surface that could potentially lead to ice fracture, yet as the reviewer mentions this approach does not explicitly provide information about the floe sizes produced by the breaking. Our model is designed to determine the size of new floes, and for this purpose we need to evaluate the strain rate criteria at each floe size and wavelength. This implies that we need to assume that all wave components interact separately with floes. Significant work would be needed to figure out how to combine the strain probability of Williams et al. (2013a) with the spectral method used in this paper, but for now, we mention this potential extension in the revised manuscript as follows:

Our approach is to determine the floe size distribution caused by the fracture of ice by surface waves, $F(\mathbf{s}, \mathbf{r})$, based on the wave spectrum. Williams et al. (2013a) used a Rayleigh distribution for the strain spectrum to predict breaking of floes, however this does not determine the floe sizes produced by the breaking. The central assumption that we will make in determining the expression for $F(\mathbf{s}, \mathbf{r})$ is that individual wave components act separately on floes.

Related to the above point: I think the Rayleigh distribution should be

$$P_{wa} = \frac{2}{\bar{a}^2} e^{-a^2/2\bar{a}^2},$$

so

$$\bar{a^2} = \int\limits_0^\infty S(\lambda) d\lambda = H_s^2/16 = \int\limits_0^\infty a^2 P_{wa} da.$$

We thank the reviewer for noticing this typo: we intended to define the Rayleigh distribution of wave amplitudes, but instead wrote the form of the distribution as if it were in terms of wave *heights*. This has been revised in the updated manuscript,

Observations of wave amplitudes (see Michel, 1999, p. 9) show wave amplitudes to be Rayleigh distributed,

$$P_{wa}(a) = \frac{8a}{H_s^2} \exp\left(-8a^2/H_s^2\right).$$

There is some additional ambiguity in the definition of $S(\lambda)$, a summary of which is found in Michel (1999), p. 3. In our first submission we chose $S(\lambda)$ to be the less-commonly-used "amplitude squared" spectrum, rather than the "half-amplitude-squared" spectrum (see our definition of a, p.2975 line 11), that appears to be more widespread. In the former case the integral of $(1/2)S(\lambda)d\lambda$ is equal to $H_s^2/16$, the same as the integral of $a^2 P_{wa}(a)$. However, to be more consistent with common notation we have updated the text to be consistent with the more common definition of $S(\lambda)$, as the "half-amplitude spectrum" in the definition of the wave amplitude (Sec. 2.3):

The amplitude of waves with wavelengths in the range λ to $\lambda + d\lambda$ is approximated following $a(\lambda) \approx \sqrt{2S(\lambda)\,d\lambda}$ (see Bouws et al. (1998), p.11, and Meylan et al. (2014), eq. 2). The spectrum $S(\lambda)d\lambda$ is equal to half the mean amplitude squared of waves belonging to waves with wavelengths between λ and $\lambda + d\lambda$, equal to the total wave energy in this wavelength band normalized by ρg.

Also, in (20), why truncate at $\lambda < r$ instead of $\lambda/2 < r$ since a wavelength of λ has maximum strain at both peaks and troughs (as the authors point out themselves)?

This is an important issue. We use a strain criteria for the ice fracturing (e.g., Dumont et al., 2011). If the ice is assumed elastic it feels the local strain rate of the wave. A

passing wave crest will therefore cause the maximum strain value to be felt at each point along the floe, and this implies that the floe fracture at each point into numerous small floes. In reality, small floes wont behave as plastic plates, therefore avoiding this problem. We therefore must choose some minimal length of a floe below which ice breaks. Our choice is somewhat arbitrary, but given the above discussion, it seems that $\lambda/2 < r$ is not much more justifiable than $\lambda < r$. It would also be difficult and arbitrary to decide, for example, in which way to fracture a floe of size $3\lambda/4$ if the criterion is based on a minimum size of $\lambda/2$, while if the minimum is λ we can just fracture each floe into two equal parts. In any case, the proper choice requires further observations and modeling, but the choice does not materially affect the model. We now explain, admittedly briefly,

> If the wavelength is larger than the floe radius, the floe is not fractured. This specification of the minimum floe size that may be fractured by a wave of wavelength λ is somewhat arbitrary, and based on the heuristic assumption that smaller floes float without being significantly strained by the waves. A better choice of this minimum floe size requires further observations and modeling.

- p2975 L1: Breaking time-scale: the authors determine it from the grid size and the wave speed. I think this is similar to using the model time step such as done by [3] or [9]. Both are somewhat artificial. [2] noticed the breaking front travelled at 0.25cg – perhaps this implies the time-scale should be ≈ 0.25 times the wave period?

We thank the reviewer for pointing out this observation, and acknowledge in the revised manuscript that this choice is affected by the lack of data on the response timescale of the ice cover to fracture by waves. We additionally performed a study of the sensitivity of the model to changes in the breaking time-scale, which we have added to the supplement in Sec. S1.3.

> The duration $\tau(\lambda)$ over which breaking occurs is approximated as the domain width divided by the group velocity for surface gravity waves,
>
> $$\tau(\lambda) = \frac{D}{c_g(\lambda)} = 2D\sqrt{\frac{2\pi}{g\lambda}}.$$
>
> Observations of wave propagation in ice (Collins et al., 2015) have suggested that the propagation speed of fracture in ice may be slower than the group velocity of surface waves. With more data, the above choice for $\tau(\lambda)$ may be re-evaluated.

Minor comments

- Is equation (4) correct? When I tried to derive it from (3) I got:

$$\partial_t \partial_r \partial_h C(\mathbf{r}, t) = \partial_t \left(\frac{f}{\pi r^2} \right)$$

$$= \frac{1}{\pi r^2} \partial_t f - \frac{2f}{\pi r^2} \partial_t r$$

$$\partial_t f = \frac{2f}{r} \partial_t r - \pi r^2 \partial_r \left(\frac{f}{\pi r^2} \partial_t r \right) - \pi r^2 \partial_h \left(f \partial_t h \right)$$

$$= \frac{4f}{r} \partial_t r - \nabla_{\mathbf{r}} \cdot (f \mathbf{G})$$

  This confusion occurred because of our previous notation, where we used $\dot{r}$ to denote rate of change of size, but this is not the same as the derivative of the size coordinate with respect to time. We changed notation throughout now such that the rate of growth of size and thickness is denoted $\mathbf{G} \equiv (G_r, G_h)$.

- Eqn (5): δ is used many times in many contexts in this paper. Perhaps reserve it for the delta function, and possibly also for the 1d function e.g. $\delta(r_p, h_p) \to \delta(r - r_p)\delta(h - h_p)$. (TC being a geophysical journal). Also perhaps define A_p nearer to (5) (there is a delay of 1 page before it's defined).

  In order to avoid confusion, we now use δ with no subscripts for delta function throughout. When we use delta to denote other quantities (e.g., width of contact zones), it is now always accompanied by an appropriate subscript. The two-dimensional delta function in Sec. 2.2 is explicitly defined now,

  > Note that the function $\delta(\mathbf{r})$ is the two-dimensional delta function: $\delta(\mathbf{r}) = \delta([r, h]) \equiv \delta(r)\delta(h)$.

- What are the limits of the integral in (15)? Is it $\int_{r_1}^{\infty} \int_{r_2}^{\infty}$ (if so it is bad notation as r1 and r2 are also the integrated variables)

  The limits are over all resolved values of r_1 and r_2, i.e. $\int_{(r_{1,min}, h_{1,min})}^{(r_{1,max}, h_{1,max})} d\mathbf{r}_1 \int_{(r_{2,min}, h_{2,min})}^{(r_{2,max}, h_{2,max})} d\mathbf{r}_2$, which becomes rather cluttered. Rather than add these definite limits, we have clarified this terminology after eq (15).

  > ... where the notation $\int_{\mathbf{r}} d\mathbf{r}$ is taken to mean an integral over all floe sizes and thicknesses resolved by the model.

- Should the left hand side of (16) be $\partial_t f$?

  It should be, we have added a second equality for clarity.

6

$$\frac{\partial f(\mathbf{r})}{\partial t} = \pi r^2 \frac{\partial N(\mathbf{r})}{\partial t} = \mathcal{L}_m(\mathbf{r}); \, (r \neq 0)$$

- p2964: $\overline{h/r} \to \overline{rh}$? (More natural to define the average using N as the weighting?)

  Since the main distribution we evolve is the FSTD, we would like to reserve the notation $\bar{x}$ as the mean with respect to the FSTD, admittedly this makes for this clunky definition of the average of a quotient.

- p2975 L19: I think the Rayleigh distribution should be

$$P_{wa} = \frac{2}{\bar{a}^2} e^{-a^2/2\bar{a}^2},$$

  See above comment, we have updated the equation to reflect the typo in Sec. 2.3 (an equation in wave amplitude instead of wave heights).

- p2975 L11: I couldn't see the "normalised energy spectrum" the authors were referring to on p11 of the WMO guide.

  Our usage of this term did not follow the WMO guide to the letter: the WMO guide refers to the "energy spectrum", though it has units m^2/Hz, so it is really the energy normalized by the water density and g (or the variance spectrum). To be consistent with the WMO guide, we avoid the term "normalized spectrum" and explain more explicitly,

  > The spectrum $S(\lambda)d\lambda$ is equal to half the mean amplitude squared of waves belonging to waves with wavelengths between λ and $\lambda + d\lambda$, equal to the total wave energy in this wavelength band normalized by ρg.

Typos

Thanks for these, they have been corrected in the revised manuscript.

- p2959, L22: have same $\to$ have the same

  Thanks, we have corrected this now,

  > assuming that all floes of different sizes have the same ITD.

- p2972, L19: the we $\to$ that we

  The sentence containing this typo has been eliminated in the revised manuscript.

Response to Comment by Reviewer #2, Luke Bennetts

1 General Comments

1. *The paper contains a lot of information. Beyond the consideration of a joint distribution, the novel contributions of the paper are not immediately apparent, e.g. novel contributions to the source terms. Therefore, I suggest a short passage at the end of the Introduction or beginning of the second section to address this.*

    Thank you for this comment, we have added a paragraph in a prominent place in the introduction section which addresses this issue.

    > The major contributions of this paper are, first, that it presents the first treatment of the *joint* floe size and thickness distribution. In addition, each of the terms in equation (2) as developed below contains a novel formulation of the corresponding process that is physically based and less heuristic than used in previous studies.

2. *The consideration of a joint distribution clearly extends the recent work of Zhang et al. (2015). However, the paper does not show the importance of the joint distribution. The paper would be much stronger if the authors provided more evidence that a joint distribution is necessary (or not). (I acknowledge the sentence on page 2977, lines 13–16.)*

    We also agree that more emphasis on this point is necessary. The paper is near a sensible length limit, which does not allow us to present additional numerical results. However, to address this point, we went through the descriptions of each of the included processes, and added relevant information to emphasize the important role of the *joint* FSTD wherever this is relevant, as follows.

    In Sec. 2.1,

    > N is the number distribution introduced above, $2\pi rh$ is the lateral area of one floe, and $\overline{2h/r}$ represents an average over all ice floes, weighted by the floe size and thickness distribution. The above result depends on the model including an explicit joint FSTD, without which this estimate for the lateral area would not be possible to obtain.

    In Sec. 3,

    > This cluster would not be resolved in a model that represented the ice thickness distribution only. The second cluster is due to a ridging interaction between floes of size I and II, leading to new floes of around 90 m size and 0.5 meters thickness. The third, due to self-interaction (ridging) between floes of size II, leads to a positive tendency at floe sizes around 17 meters and thickness around 1.7 meters. Both the second and third clusters of floes would not be resolved in a model that represents the floe size distribution only, showing again the importance of representing the joint FSTD.

In Sec. 2.3,

> We note again that the distribution of both floe size and thicknesses plays a critical role in determining the fracture of ice by waves, underlying the need to use the coupled FSTD for representing the effects of ice fracture due to surface waves.

2   Specific Comments

1. The model appears to be designed for the marginal ice zone. I think this should be explicitly stated, e.g. in the title of the paper.

   While we prefer not to alter the title of the paper, we made more explicitly clear in the abstract, introduction, and conclusion the applicability of the model to the MIZ. Specifically, in the abstract:

   > [Sea ice] is characterized by a complex and continuously changing distribution of floe sizes and thicknesses, particularly in the marginal ice zone (MIZ).

   > The model accounts for effects due to multiple processes that are active in the MIZ: freezing and melting along the lateral side and base of floes, mechanical interactions due to floe collisions (ridging and rafting) and sea-ice fracture due to swell propagation in the MIZ and at the ice margin.

   The introduction now includes

   > The most dramatic intra-annual variability in sea ice cover is found in the MIZ, and in seasonal ice zones, regions which range from being ice-covered to ice-free over the year. As sea-ice cover becomes thinner and more fractured, these regions will become larger, and the distribution of these floes and their size, shape, and properties may change.

   The conclusion now includes

   > We developed a model that simulates the evolution of the FSTD, using as input large-scale oceanic and atmospheric forcing fields, which may be useful as an extension to sea-ice models presently used in global climate models, in particular in regions with a continuously varying FSTD, such as the marginal ice zone.

2. Page 2957, top: The marginal ice zone is often defined as the part of the ice-covered ocean where ocean waves cause ice breakage (see Weeks (2010) and more recently Williams et al. (2013a,b)).

   We agree, since there are two definitions of the MIZ, we have added text that addresses this point.

> . . . the Arctic marginal ice zone, defined as either the region of the ocean over which ice waves lead to the fracture of ice (e.g. Williams et al., 2013b), or as the area of ice with concentration between 15% and 80%, has been widening during the summer season (Strong and Rigor, 2013).

3. Page 2957, line 5: The recent publication Kohout et al. (2015) could be cited here. We agree, and have added a reference at this suggested place in the introduction.

> (Asplin et al., 2012; Zhang et al., 2013; Kohout et al., 2015)

More discussion of this paper has been included in other relevant locations. Specifically, in the development of the mechanical component,

> Observations (Collins et al., 2015; Kohout et al., 2015) have indicated that floes may break up along ridges, in which case equation (18) may be used to provide information about the time evolution of ridging or ridge density. This is is a potential future extension of the present work.

4. Page 2957, line 15 onwards: Definite statements would help here. For instance, Steele (1992) showed that lateral melting is important for floes of a 30 m diameter or less. We agree that further clarification is necessary, and have provided it in the introduction.

> The fractured sea-ice cover has increased floe perimeter, which may lead to enhanced melting and a more rapid reduction in sea-ice area compared to an unfractured sea-ice cover. Steele (1992) indeed demonstrated an increasing sensitivity of the ice cover to lateral melting with decreasing floe size, finding that below 30 m lateral melting was critically important. Smaller floe sizes may additionally lead to changes in the mechanical response of the sea-ice cover to forcing from the ocean and atmosphere, as floe size is a parameter in collisional models of ice rheology (Shen et al., 1986, 1987; Feltham, 2005, 2008).

5. The statement "level of detail may not suffice... where the ice cover is heterogeneous..." on page 2958, line 23 seems odd considering the statement that "sea ice is heterogeneous" on page 2957, line 7. We agree that this wording is a bit clumsy, and so we have clarified the text as follows,

> Modern approaches to modeling sea ice in GCMs, such as the community ice model (Hunke et al., 2013), generally approximate ice cover as a non-Newtonian fluid with a vertically layered thermodynamics, and simple thickness distribution (Thorndike et al., 1975; Semtner, 1976; Hibler, 1979). This approximation may not suffice, because it does not account for the distribution of floe sizes and therefore for the above mentioned related effects.

We have additionally moved the reference to Birnbaum and Lüpkes (2002) to earlier in the introduction, and removed the reference to Girard et al. (2009) as it is no longer relevant to the discussion where it was cited,

Floe sizes can also affect the surface drag coefficient and therefore air-sea fluxes (Birnbaum and Lüpkes, 2002).

6. Page 2959, line 5: Please quantify the 'large observation window' and 'point observations'.

We have removed the discussion of truncation error with respect to FSD measurements, where the text "large observational window" appears, deciding that this is not necessary given manuscript length limits. We have also clarified the meaning of "point observations" in the text to be reflect the location of the measurements that were made,

> In spite of these challenges, many observations of the floe size distribution have been made, often using helicopter or ship-board cameras, notably in the Alaskan and Russian Arctic (Holt and Martin, 2001), Sea of Okhotsk (Toyota and Enomoto, 2002; Toyota et al., 2006), Prydz Bay (Lu et al., 2008), and Weddell Sea (Herman, 2010; Toyota et al., 2011).

7. Page 2959, lines 19–20: Dumont et al. (2011) and Williams et al. (2013a,b) focussed on wave attenuation and wave-induced ice breakage. It would be useful to add a short discussion of the relationship between these investigations and the study presented in this paper.

We agree that further discussion and comparison may be useful, and included information about other models of the FSD. We have updated the introduction to include more discussion of both papers.

> Other modeling studies involving the temporal evolution of the floe size distribution have mainly focused on understanding ocean wave propagation and attenuation in the marginal ice zone (Dumont et al., 2011; Williams et al., 2013a,b), who developed spectral models of ocean wave propagation, attenuation, and associated ice breakage. Both studies modeled the FSD using the renormalization group method of Toyota et al. (2011).

We have additionally updated Sec. 2.3 to include a discussion of the model presented by Williams et al. (2013a).

> Williams et al. (2013a) used a Rayleigh distribution for the strain spectrum to predict breaking of floes, however this does not determine the floe sizes produced by the breaking. The central assumption that we will make in determining the expression for $F(\mathbf{s}, \mathbf{r})$ is that individual wave components act separately on floes.

> This approach may be compared with the spectral method of Williams et al. (2013a), where the fracture probability is extended, by assuming that the ice strain is Rayleigh distributed, and the size distribution of new floes is determined using the renormalization group method of Toyota et al. (2011), with a maximum floe size equal to half of the wavelength that corresponds to the zero-crossing period.

8. Page 2960, following equation 2: Please define the Laplacian operator and the physical domain.

We now do this.

> ... where $\mathbf{r} = (r, h)$, and $\nabla = (\frac{\partial}{\partial x}, \frac{\partial}{\partial y})$ is the two-dimensional Laplacian. The two dimensional spatial domain may be thought of as corresponding to a single grid cell of a climate model, on the order of tens of km on a side.

9. Section 2.2, paragraph 1: Can the floes rebound following a collision and/or cause erosion of the floe edges?

This is not a feature of the model, though this is an important phenomenon. When floes interact, they are assumed to combine with each other. We have added a sentence to this effect.

> In reality, some floe collisions may lead to a rebound and erosion of floe edges rather than to a merging of the floes, yet we do not account for such a process.

10. Page 2965, lines 21–23 to page 2966, lines 1–4: This long sentence is unclear and should be rewritten.

We have rewritten these lines for clarity. The first part has been updated to read:

> The integral of $f(\mathbf{r})$ over all floe sizes and thicknesses, including open water, is equal to one. Therefore, ignoring thermodynamic and wave effects, we integrate (2) over a range of floe sizes that includes a vanishingly small interval of sizes around $\mathbf{r} = (r, h) = \mathbf{0}$,

The second sentence referred to by the reviewer has been updated to read:

> The integral of $f(\mathbf{r})$ over all floe sizes and thicknesses, but excluding open water ($\mathbf{r} = 0$), is equal to the ice concentration, c. Integrating (2) as before but now excluding $\mathbf{r} = \mathbf{0}$,

11. Page 2971, lines 1–2: What is the physical basis for the collision probability? It does not appear to be based on dynamical considerations, e.g. the strength of the prevailing winds and/or waves. Herman (2011, 2013), Shen and Squire (1998) and Fig. 10 of Bennetts and Williams (2015) may be useful for future developments of this aspect of the model.

We thank the reviewer for bringing up this point, and also for the reference to Bennetts and Williams (2015). We now explain in Sec. 2.2.1,

> The above probability that two floes will collide is based on geometric constraints. However, the rate of collisions depends also on the ice strain rate tensor $\dot{\boldsymbol{\epsilon}}$ as explained above, and this tensor depends on external forcings such as the strength of the prevailing winds and currents (Shen et al., 1987;

Herman, 2011, 2013; Bennetts and Williams, 2015), but the determination of that relationship is not a focus of the FSTD model presented here.

12. Page 2973, line 10: I suggest not referring to 'wave-breaking' here, as it is already reserved for a different phenomenon.

We agree, and wherever appropriate we have updated the text to be more specific. In the beginning of the Sec. 2.3, we have updated two lines:

the response of the FSTD to fracture by waves

and

The rate of change of area of floes of size $\mathbf{r}$ due to fracture by ocean surface waves is then,

13. Page 2974, paragraph 2: Kohout and Meylan (2008)'s wave attenuation model based on scattering is important and should be cited. However, the model has progressed since then. In particular, Vernon Squire and I derived a semi-analytic expression for the attenuation coefficient (Bennetts and Squire, 2012a). Moreover, we approximated the functional dependencies of the attenuation coefficient for applications such as the one presented in this paper (Bennetts and Squire, 2012b). I also suggest adding a statement that Kohout and Meylan (2008)'s Fig. 6 assumes the floes are long, and that the attenuation rate tends to zero as the floes become shorter (see their Fig. 3 and Figs. 6–7 of Bennetts and Squire (2012a)). Of greater significance, Kohout and Meylan (2008), Bennetts et al. (2010) and Bennetts and Squire (2012b) showed that scattering models significantly under predict measured attenuation rates. Thus, using a scattering-attenuation model alone allows long waves to cause ice breakage unrealistically far into the ice-covered ocean (Williams et al., 2013b).

We have implemented the model of Bennetts and Squire (2012) alongside with the attenuation coefficient of Kohout and Meylan (2008), and now explain,

Scattering models may under-predict attenuation rates (Williams et al., 2012), which may allow for longer penetration of waves into the MIZ than is physically realistic. Updated models of the wave attenuation (Bennetts and Squire, 2012) suggest different attenuation coefficients as function of wave period and ice thickness. We tested our model with the Bennetts and Squire (2012) attenuation coefficient, and show in the supplement (Sec. S1.3), that our FSTD model can be sensitive to the choice of attenuation model. Future applications of this FSTD model should therefore carefully consider the wave attenuation formulation, based on both model estimates and observations (e.g., Meylan et al., 2014) .

In addition, when describing the elastic plate model in Sec, 3.2, we have added, as suggested,

Kohout and Meylan (2008) modeled floes as long floating elastic plates

13

14. Page 2974, line 19: The statement 'wave fracture depends on their wavelengths rather than periods' is not strictly correct.

This is true, and we have updated the text of Sec. 2.3 to reflect this,

> We convert the attenuation coefficients, reported as a function of wave period, to a function of wavelength using the deep-water surface gravity wave dispersion relation, $\lambda = gT^2/2\pi$.

15. Page 2975: How does the spectral model differ to that of Williams et al. (2013a)?

We added such a discussion both in the introduction and in Sec. 2.3. Specifically, in the introduction:

> Other modeling studies involving the temporal evolution of the floe size distribution have mainly focused on understanding ocean wave propagation and attenuation in the marginal ice zone (Dumont et al., 2011; Williams et al., 2013a,b). These studies developed models of ocean wave propagation, attenuation and associated ice breakage, and modeled the FSD using the renormalization group method of Toyota et al. (2011).

In the ice fracture section:

> Our approach is to determine the floe size distribution caused by the fracture of ice by surface waves, $F(\mathbf{s}, \mathbf{r})$, based on the wave spectrum. Williams et al. (2013a) used a Rayleigh distribution for the strain spectrum to predict breaking of floes, however this does not determine the floe sizes produced by the breaking.

16. Page 2977, lines 18–20: Note that Williams et al. (2013a) extended the expression for the critical failure limit, and Williams et al. (2013b) showed the width of region of broken ice predicted by their model could be highly sensitive to this parameter (Section 5.2).

Thank you, we now note this possible extension to the simpler formulation we use (Sec. 3).

> The critical strain amplitude for flexural failure, ϵ_{crit}, is set to 3×10^{-5} in line with other studies (Kohout and Meylan, 2008; Dumont et al., 2011). Williams et al. (2013a) formulated a more complex expression for the critical failure limit, and this was found to have a significant effect on wave fracturing (Williams et al., 2013b). We examine the model sensitivity to some of the main parameters used in these model simulations in the supplement (Sec. S1).

17. Section 3: Have convergence and sensitivity tests been conducted?

We would like to thank the reviewer for this suggestions: in response to this suggestion we performed a set of numerical convergence and sensitivity tests, which are now included as supplementary material as Sec. S1 (sensitivity) and Sec. S2 (convergence),

for major model parameters. In doing so we uncovered a bug in the advection scheme that was used to describe the thermodynamic growth and melting of floes, which we are happy to have found. As a consequence, we have separated the former model variables r_p, which was the "pancake floe size", into two variables r_min, which is the minimum resolved floe size, and r_lw, which is the width of the lead region, to examine the sensitivity to their use independently. We have additionally changed h_p to h_min. These changes appear in Sec. 2.1,

> The lead region is defined as the annulus around each floe of width r_lw ...

> If the water is at its freezing point, a cooling heat flux leads to freezing of pancakes of ice of radius r_min and thickness h_min ...

The sensitivity studies are mentioned in Sec. 3,

> We examine model sensitivity to the parameter choices used in these model runs in the supplement (Sec. S1).

Additionally, when discussing the discretization, we note

> We examine the numerical convergence of the model in the supplement (Sec. S2) finding that increasing this resolution does not alter the numerical results.

18. Section 4: The opening paragraph doesn't seem appropriate for a Conclusions section.

    We agree, and so we have deleted this paragraph.

19. Page 2981, lines 21–22: Have the forcing fields been considered 'when combined'?

    This sentence has been removed, thanks!

Technical Corrections Thanks for these corrections, they have all been addressed in the revised manuscript.

1. Page 2961, line 13: Separate the equation from the text.

    We have separated the equation.

    > The cumulative number distribution is defined as

    $$C(\mathbf{r}) = \int\limits_0^\mathbf{r} N(\mathbf{r'})\ d\mathbf{r'} = \int\limits_0^\mathbf{r} (f(\mathbf{r'})/\pi r'^2)\ d\mathbf{r'}, \dots$$

2. Page 2972, line 19: Delete 'the'.

    We have deleted it, thanks for catching this!

3. Page 2977, line 7: 'Wave fracture' → 'ice fracture' or 'wave-induced fracture'.

In all places with this phrase, we have changed it to either "fracture of ice floes due to surface waves", or some variant.

In Sec. 2.3,

> ... $\mathcal{L}_W(\mathbf{r})$ is the time rate of change of floes of size and thickness $\mathbf{r} = (r, h)$ due to fracture of ice by surface waves ... the response of the FSTD to ice fracture by waves ...

> Our approach is to determine the floe size distribution caused by the fracture of ice by surface waves ...

> ... representing the effects of ice fracture due to surface waves.

> The effects of the fracture of ice by waves ... the effects of ice fracture by waves ...

In Sec. 3,

> ... leading to ice fracture.

> Ice at this size and thickness is susceptible to fracture by surface waves ... not susceptible to fracture ...

> Ice thickness does not change when the ice is fractured.

> ... simulates a seven-day period of ice fracture by surface waves ...

In the caption for Fig. 3,

> Change in response to wave forcing only ...

In the caption for Fig. 5,

> ... one week of ice fracture by surface waves with the specified wave spectrum.

In Table 4,

> Ice fracture component of FSTD model.

> ... fracture of floes of size $\mathbf{r}$ by waves.

> Variables used in the representation of the fracture of ice by surface waves in the FSTD model.

4. Figure 3's caption appears to be incorrect with respect to the labelling.

This has been updated to fix the typo.

References

Asplin, M. G., Galley, R., Barber, D. G., and Prinsenberg, S.: Fracture of summer perennial sea ice by ocean swell as a result of Arctic storms, J. Geophys. Res., 117, 1–12, doi: 10.1029/2011JC007221, 2012.

Bennetts, L. G. and Squire, V. a.: Model sensitivity analysis of scattering-induced attenuation of ice-coupled waves, Ocean Modelling, 45-46, 1–13, doi:10.1016/j.ocemod.2012.01.002, 2012.

Bennetts, L. G. and Williams, T. D.: Water wave transmission by an array of floating disks, Proc. Roy. Soc. A, 471, 1–18, doi:10.1098/rspa.2014.0698, 2015.

Birnbaum, G. and Lüpkes, C.: A new parameterization of surface drag in the marginal sea ice zone, Tellus A, 54, 107–123, doi:10.1034/j.1600-0870.2002.00243.x, 2002.

Bouws, E., Draper, L., Shearman, E., Laing, A., Feit, D., Mass, W., Eide, L., Francis, P., Carter, D., and Battjes, J.: Guide to Wave analysis and forecasting, World Meteorological Organization, 1998, 11–12, 1998.

Collins, C. O., Rogers, W. E., Marchenko, A., and Babanin, A. V.: In situ measurements of an energetic wave event in the Arctic marginal ice zone, Geophys. Res. Lett., 42, 1863–1870, doi:10.1002/2015GL063063, 2015.

Dumont, D., Kohout, A., and Bertino, L.: A wave-based model for the marginal ice zone including a floe breaking parameterization, J. Geophys. Res., 116, C04 001, doi:10.1029/2010JC006682, 2011.

Feltham, D. L.: Granular flow in the marginal ice zone., Philosophical transactions. Series A, Mathematical, physical, and engineering sciences, 363, 1677–1700, doi:10.1098/rsta.2005.1601, 2005.

Feltham, D. L.: Sea Ice Rheology, Annual Review of Fluid Mechanics, 40, 91–112, doi:10.1146/annurev.fluid.40.111406.102151, 2008.

Girard, L., Weiss, J., Molines, J. M., Barnier, B., and Bouillon, S.: Evaluation of high-resolution sea ice models on the basis of statistical and scaling properties of Arctic sea ice drift and deformation, J. Geophys. Res., 114, C08 015, doi:10.1029/2008JC005182., 2009.

Herman, A.: Sea-ice floe-size distribution in the context of spontaneous scaling emergence in stochastic systems, Phys. Rev. E., 81, 066 123, doi:10.1103/PhysRevE.81.066123, 2010.

Herman, A.: Molecular-dynamics simulation of clustering processes in sea-ice floes, Physical Review E, pp. 1–25, 2011.

Herman, A.: Numerical modeling of force and contact networks in fragmented sea ice, Annals of Glaciology, 54, 114–120, doi:10.3189/2013AoG62A055, 2013.

Hibler, W. D.: A Dynamic Thermodynamic Sea Ice Model, J. Phys. Oceanogr., 9, 815–846, doi:10.1175/1520-0485(1979)009⟨0815:ADTSIM⟩2.0.CO;2, 1979.

Holt, B. and Martin, S.: The effect of a storm on the 1992 summer sea ice cover of the Beaufort, Chukchi, and East Siberian Seas, J. Geophys. Res., 106, 1017, doi:10.1029/1999JC000110, 2001.

Hunke, E. C., Lipscomb, W. H., Turner, A. K., Jeffery, N., and Elliot, S.: CICE: The Los Alamos Sea Ice Model Documentation and SoftwareUsers Manual Version 5.0, Tech. rep., Los Alamos Natl. Laboratory, Los Alamos, N.M., 2013.

Kohout, A., Williams, M., Toyota, T., Lieser, J., and Hutchings, J.: In situ observations of wave-induced sea ice breakup, Deep Sea Research Part II: Topical Studies in Oceanography, pp. 1–6, doi:10.1016/j.dsr2.2015.06.010, 2015.

Kohout, A. L. and Meylan, M. H.: An elastic plate model for wave attenuation and ice floe breaking in the marginal ice zone, J. Geophys. Res., 113, C09 016, doi:10.1029/2007JC004434, 2008.

Lu, P., Li, Z. J., Zhang, Z. H., and Dong, X. L.: Aerial observations of floe size distribution in the marginal ice zone of summer Prydz Bay, J. Geophys. Res., 113, C02 011, doi:10.1029/2006JC003965, 2008.

Meylan, M. H., Bennetts, L. G., and a. L. Kohout: In situ measurements and analysis of ocean waves in the Antarctic marginal ice zone, Geophys. Res. Lett., 41, 1–6, doi:10.1002/2014GL060809.In, 2014.

Michel, W. H.: Sea Spectra Revisited, Mar Technol, 36, 211–227, 1999.

Semtner, A. J.: A Model for the Thermodynamic Growth of Sea Ice in Numerical Investigations of Climate, J. Phys. Oceanogr., 6, 379–389, doi:10.1175/1520-0485(1976)006⟨0379:AMFTTG⟩2.0.CO;2, 1976.

Shen, H., Hibler, W., and Leppäranta, M.: On applying granular flow theory to a deforming broken ice field, Acta Mechanica, 6Shen, H.,, 143–160, doi:10.1007/BF01182545, 1986.

Shen, H. H. and Sankaran, B.: Internal Length And Time Scales In A Simple Shear Granular Flow, Physical Review E, 70, 51 308, doi:10.1103/PhysRevE.70.051308, 2004.

Shen, H. H., Hibler, W. D., and Leppäranta, M.: The role of floe collisions in sea ice rheology, Journal of Geophysical Research, 92, 7085, doi:10.1029/JC092iC07p07085, 1987.

Steele, M.: Sea ice melting and floe geometry in a simple ice-ocean model, J. Geophys. Res., 97, 17 729, doi:10.1029/92JC01755, 1992.

Strong, C. and Rigor, I. G.: Arctic marginal ice zone trending wider in summer and narrower in winter, Geophys. Res. Lett., 40, 4864–4868, doi:10.1002/grl.50928, 2013.

Thorndike, A. S., Rothrock, D. A., Maykut, G. A., and Colony, R.: The thickness distribution of sea ice, J. Geophys. Res., 80, 4501, doi:10.1029/JC080i033p04501, 1975.

Toyota, T. and Enomoto, H.: Analysis of sea ice floes in the Sea of Okhotsk using ADEOS/AVNIR images, in: Proceedings of the 16th IAHR International Symposium on Ice, pp. 211–217, International Association of Hydraulic Engineering and Research, 2002.

Toyota, T., Takatsuji, S., and Nakayama, M.: Characteristics of sea ice floe size distribution in the seasonal ice zone, Geophys. Res. Lett., 33, L02 616, doi:10.1029/2005GL024556, 2006.

Toyota, T., Haas, C., and Tamura, T.: Size distribution and shape properties of relatively small sea-ice floes in the Antarctic marginal ice zone in late winter, Deep-Sea Res. II, 58, 1182–1193, doi:10.1016/j.dsr2.2010.10.034, 2011.

Williams, T. D., Bennetts, L. G., and Squire, V. a.: Wave-ice interactions in the marginal ice zone : model sensitivity studies along a 1-D section of the Fram Strait, Ocean Model., 2012.

Williams, T. D., Bennetts, L. G., Squire, V. a., Dumont, D., and Bertino, L.: Waveice interactions in the marginal ice zone. Part 1: Theoretical foundations, Ocean Model., 71, 81–91, doi:10.1016/j.ocemod.2013.05.010, 2013a.

Williams, T. D., Bennetts, L. G., Squire, V. A., Dumont, D., and Bertino, L.: Wave-ice interactions in the marginal ice zone. Part 2: Numerical implementation and sensitivity studies along 1D transects of the ocean surface, Ocean Modelling, 71, 92–101, doi:10.1016/j.ocemod.2013.05.011, 2013b.

Zhang, J., Lindsay, R., Schweiger, A., and Steele, M.: The impact of an intense summer cyclone on 2012 Arctic sea ice retreat, Geophys. Res. Lett., 40, 720–726, doi:10.1002/grl.50190, 2013.

Zhang, J., Schweiger, A., Steele, M., and Stern, H.: Sea ice floe size distribution in the marginal ice zone: Theory and numerical experiments, Journal of Geophysical Research: Oceans, 120, 3484—-3498, doi:10.1002/2015JC010770, 2015.

A prognostic model of the sea ice floe size and thickness distribution

Christopher Horvat[1] and Eli Tziperman[1]

[1]School of Engineering and Applied Sciences and Department of Earth and Planetary Sciences, Harvard University, Cambridge, MA, USA

Correspondence to: Christopher Horvat (horvat@fas.harvard.edu)

Abstract. Sea ice exhibits considerable seasonal and longer-term variations in extent, concentration, thickness and age, and is characterized by a complex and continuously changing distribution of floe sizes and thicknesses, particularly in the marginal ice zone (MIZ). Models of sea ice used in current climate models keep track of its concentration and of the distribution of ice thicknesses, but do not account for the floe size distribution and its potential effects on air-sea exchange and sea-ice evolution. Accurately capturing sea-ice variability in climate models may require a better understanding and representation of the distribution of floe sizes and thicknesses. We develop and demonstrate a model for the evolution of the joint sea-ice floe size and thickness distribution that depends on atmospheric and oceanic forcing fields. The model accounts for effects due to multiple processes that are active in the ~~marginal~~ MIZ and seasonal ice zones: freezing and melting along the lateral side and base of floes, mechanical interactions due to floe collisions (ridging and rafting) and sea-ice fracture due to ~~swell propagation into the ice pack~~ wave propagation in the MIZ. The model is then examined and demonstrated in a series of idealized test cases.

1 Introduction

Sea ice is a major component of the climate system, covering about 12% of the ocean surface. It drives the ice-albedo feedback, a potential source of climate instability and polar amplification, and it affects deep water formation and air-sea fluxes of heat, fresh water and momentum between the atmosphere and ocean. Its presence also provides a platform for high-latitude ecosystems and determines polar shipping routes. Additionally, sea ice is well-correlated with patterns of atmospheric variability such as the North Atlantic Oscillation (Strong et al., 2009), the Antarctic Oscillation (Wu and Zhang, 2011), and the Madden-Julian Oscillation (Henderson et al., 2014). Over the past

few decades, Arctic sea ice has become thinner, less extensive, and more seasonal (Cavalieri and Parkinson, 2012). Regions that were once covered by ice year-round now are ice-free in the summer (Stroeve et al., 2012), and the Arctic marginal ice zone, defined as ~~the~~ either the region of the ocean over which waves lead to the fracture of ice (e.g. Williams et al., 2013b) , or as the area of ice with concentration between 15% and 80%, which has been widening during the summer season (Strong and Rigor, 2013). High-latitude storms are capable of breaking thinning pack ice into smaller floes, changing ocean circulation and air-sea exchange ~~(Asplin et al., 2012; Zhang et al., 2013)~~ (Asplin et al., 2012; Zhang et al., 2013; Ko with evidence suggesting that these storms will become more prevalent in the future (Vavrus et al., 2012).

Sea-ice cover is heterogeneous, composed of a distribution of floes of different areas and thicknesses. Floes can vary dramatically in size, ranging from newly-formed frazil crystals millimeters in size to pack ice in the Canadian Arctic with floes up to ten meters thick in places and hundreds of kilometers wide. ~~As~~ The most dramatic intra-annual variability in sea ice cover is found in the MIZ, and in seasonal ice zones, regions which range from being ice-covered to ice-free over the year. As summer sea-ice cover becomes thinner and more fractured, these regions will become larger, and the distribution of these floes and their size, shape, and properties may change. Events that generate surface waves, such as a fortuitously observed Arctic cyclone in 2011, the so-called "Great Arctic Cyclone" of 2012, and an energetic wave event observed in the Barents sea, can lead to the fracturing of floes (Asplin et al., 2012; Zhang et al., 2013; Collins et al., 2015). The fractured sea-ice cover has increased floe perimeter, which may lead to enhanced melting and a more rapid reduction in sea-ice area compared to an unfractured sea-ice cover~~(Steele, 1992) , and may~~ . Steele (1992) indeed demonstrated an increasing sensitivity of the ice cover to lateral melting with decreasing floe size, finding that below 30 m lateral melting was critically important. Smaller floe sizes may additionally lead to changes in the mechanical response of the sea-ice cover to forcing from the ocean and atmosphere~~(Feltham, 2005)~~, as floe size is a parameter in collisional models of ice rheology (Shen et al., 1986, 1987; Feltham, 2005, 2008) . As sea ice attenuates wave energy, the diminished ice fraction may lead to further surface wave propagation into the ice field, enhancing fracturing farther from the sea-ice edge, and leading to further sea-ice area loss in a positive feedback loop ~~(Asplin et al., 2014) .~~ (Asplin et al., 2014) . Floe sizes can also affect the surface drag coefficient and therefore air-sea fluxes (Birnbaum and Lüpkes, 2002) . Along floe edges, ocean eddies may be generated due to the gradient in surface heat and stress boundary conditions between ice edge and open water (Niebauer, 1982; Johannessen et al., 1987). These eddies may more rapidly mix air-sea heat flux absorbed by open water to underneath sea-ice floes when floe sizes are comparable to the eddy length scale, but not when floe sizes are much larger. This in turn may have consequences for ice melt rates and ocean circulation (Horvat and Tziperman, 2014).

Given that it is not computationally practical to simulate all individual floes, properties of the ice cover can instead be described using statistical distributions. This approach was pioneered by

2

Thorndike et al. (1975), who developed a framework for simulating the thickness distribution (ITD), $g(h)$, defined such that $g(h)dh$ is the fractional area of the sea surface covered by ice with thickness between h and $h + dh$. The Thorndike model evolves the prognostic equation

$$\frac{\partial g(h)}{\partial t} = -\nabla \cdot (g\,\mathbf{u}) - \frac{\partial}{\partial h}(g(h)G_h) + \psi, \tag{1}$$

where $\mathbf{u}$ is the horizontal ice velocity, ~~$\dot{h}$~~ G_h is the rate of change of ice thickness due to melting and freezing (thermodynamics), and ψ, the "redistribution function", describes the creation of ice of thickness h by mechanical combination of ice of different thicknesses. Measurements of ice thickness are made possible by a variety of remote sensing techniques such as submarine sonar, fixed moorings, helicopter borne electromagnetic induction, and satellite measurements (Bourke and Garrett, 1987; Yu and Rothrock, 1996; Renner and Gerland, 2014), which may be used to test model skill. Variants of the Thorndike model have been implemented in several general circulation models (GCMs, Bitz, 2008; Hunke et al., 2013), and have been used to understand sea ice behavior and predictability (Bitz et al., 2001; Chevallier and Salas-Mélia, 2012).

Modern approaches to modeling sea ice in GCMs, such as the community ice model (Hunke et al., 2013), generally approximate ice cover as a non-Newtonian fluid with a vertically layered thermodynamics, and simple thickness distribution (Thorndike et al., 1975; Semtner, 1976; Hibler, 1979). This ~~level of detail~~ approximation may not suffice ~~in regions where ice cover is heterogeneous and variable (Birnbaum and Lüpkes, 2002; Girard et al., 2009) , as~~ , because it does not account for the ~~lateral size distribution of floes~~ distribution of floe sizes and therefore for the above mentioned related effects.

We aim to describe the sub-grid scale variability of the sea-ice cover by extending the ice thickness distribution to a joint distribution that includes both ice thickness and floe size. Rothrock and Thorndike (1984) were among the first to describe the distribution of lateral floe sizes, defining the floe size distribution (FSD) $n(r)\,dr$ as the fractional area of the sea surface covered by floes with lateral size between r and $r + dr$. The size of a floe with area a is represented by its effective radius, $r = \sqrt{a/\pi}$, which represents floes as cylinders of radius r. Modeling of the lateral floe size distribution is hampered by the difficulty of measurement, as floe sizes vary over many orders of magnitude. ~~Such physical systems require a large observational window in order to avoid truncation errors that under-sample large elements (Lu et al., 2008) .~~ Even with sufficient imagery, algorithms that identify and measure floes must overcome many obstacles, such as submerged floes, melt ponds, and clouds. In spite of these challenges, many ~~point~~ observations of the floe size distribution have been ~~successfully~~ made, often using helicopter or ship-board cameras ~~(Holt and Martin, 2001; Toyota and Enomoto, 2002; Toyota et al., 2006; Lu et al., 2008; Herman, 2010; Toyota et al., 2011) ,~~ notably in the Alaskan and Russian Arctic (Holt and Martin, 2001) , Sea of Okhotsk (Toyota and Enomoto, 2002; Toyota et al., 2006) , Prydz Bay (Lu et al., 2008) , and Weddell Sea (Herman, 2010; Toyota et al., 2011) . These studies have focused on deriving and fitting scaling relationships measured distributions, leading to power-

law (Toyota et al., 2006), Pareto (Herman, 2010), or joined power-law (Toyota et al., 2011) distributions of floe sizes. The temporal evolution of the floe size distribution has been examined in a small number of observational studies (Holt and Martin, 2001; Steer et al., 2008; Perovich and Jones, 2014), that analyzed the change in the floe size distribution over several weeks or seasonally, but these observations, particularly in the marginal ice zone, are limited. ~~Analytic studies involving the evolution of the floe size distribution have mainly focused on understanding ocean wave propagation and attenuation in the marginal ice zone (Dumont et al., 2011; Williams et al., 2013a) .~~

Herman (2010) modeled the FSD as a generalized Lotka-Volterra system, which admits as a solution a Pareto distribution of floe sizes, and suggested that this distribution might fit observed FSDs. Toyota et al. (2011) showed that observed FSDs in the Weddell Sea may be fit by a power law and, that such a scaling relationship may be obtained by assuming that ice fracture is a self-similar process, following a renormalization group method. Zhang et al. (2015) developed a model ~~to simulate~~ for the floe size distribution evolution, assuming that all floes of different sizes have the same ITD. The present paper, however, develops a model for the *joint* floe size and thickness distribution, allowing for different ice thickness distribution for each horizontal size class. The Zhang et al. (2015) paper shares many of our goals and we refer to it below, further elaborating on additional differences between the two studies in the treatment of thermodynamics, mechanical interactions and wave fracturing. Other modeling studies involving the temporal evolution of the floe size distribution have mainly focused on understanding ocean wave propagation and attenuation in the marginal ice zone (Dumont et al., 2011; Williams et al., 2013a, b) . These studies developed models of ocean wave propagation, attenuation and associated ice breakage, and modeled the FSD using the renormalization group method of Toyota et al. (2011) .

The purpose of the present paper is to develop and demonstrate a framework for modeling the joint distribution of floe sizes and thicknesses (referred to below as the FSTD) $f(r,h)$, with $f(r,h) \, dr \, dh$ being the fraction of the ocean surface area covered by floes of thickness between h and $h + dh$ and lateral size between r and $r + dr$ (a list of variable names and descriptions are provided in Table 1). The ice thickness distribution $g(h)$ and floe size distribution $n(r)$ are obtained by integrating over the joint distribution $f(r,h)$,

$$g(h) = \int_0^\infty f(r,h) \, dr,$$

$$n(r) = \int_0^\infty f(r,h) \, dh.$$

The prognostic equation for the joint floe size and thickness distribution has the form,

$$\frac{\partial f(\mathbf{r})}{\partial t} = -\nabla \cdot (f(\mathbf{r}) \, \mathbf{u}) + \mathcal{L}_T + \mathcal{L}_M + \mathcal{L}_W, \tag{2}$$

where $\mathbf{r} = (r,h)$~~. The~~, and $\nabla = (\frac{\partial}{\partial x}, \frac{\partial}{\partial y})$ is the two-dimensional Laplacian. The two dimensional spatial domain may be thought of as corresponding to a single grid cell of a climate model, on the

4

order of tens of km on a side. The term $\nabla \cdot (f(\mathbf{r})\,\mathbf{u})$ describes advection of the floe size distribution
130 by the flow of ice. $\mathcal{L}_T$ is the time rate of change of the floe size distribution due to thermodynamic
effects. $\mathcal{L}_M$ is the time rate of change due to mechanical interaction (rafting and ridging of floes).
$\mathcal{L}_W$ is the time rate of change due to floes being fractured by surface ocean waves. We parameterize
each of the above processes, forced by grid-scale atmospheric and oceanic forcing fields. The major
contributions of this paper are, first, that it presents the first treatment of the *joint* floe size and
135 thickness distribution. In addition, each of the terms in equation (2) as developed below contains a
novel formulation of the corresponding process that is physically based and less heuristic than used
in previous studies.

The paper proceeds as follows: we first develop explicit representations for the different processes
affecting the joint floe size and thickness distribution in response to atmospheric and oceanic forcing
140 ~~(section 2)~~in section 2. The model response to individual forcing fields, in the form of air-sea heat
fluxes, ice flow that leads to floe collisions, and surface waves, is analyzed in section 3. We conclude
in section 4.

2 Representing processes that affect the joint floe size and thickness distribution

2.1 Thermodynamics

145 Air-sea heat fluxes in the polar oceans lead to the freezing and melting of ice. In regions of open
water, cooling produces frazil ice which may consolidate with other floes or form pancakes. When
floes grow due to the accumulation of frazil crystals, or by congelation growth at their bases, their
size and thickness will change, but the total number of floes will not. Suppose that the only source or
sink of ice volume is due to freezing and melting of existing floes, which causes them to change their
150 size at a rate we denote as G_r and thickness at a rate $\mathbf{G} = (\dot{r}, \dot{h}) G_h$, and we define $\mathbf{G} \equiv (G_r, G_h)$. Let
N be the number distribution, such that $N(\mathbf{r})\,dh\,dr$ is the number of floes in the range $(h, h+dh)$,
$(r, r+dr)$ (a list of the variables used to describe FSTD thermodynamics is provided in Table 2).
The cumulative number distribution is defined as $C(\mathbf{r}) = \int_0^{\mathbf{r}} N(\mathbf{r}')\,d\mathbf{r}' = \int_0^{\mathbf{r}} (f(\mathbf{r}')/\pi r'^2)\,d\mathbf{r}',$

$$C(\mathbf{r}) = \int_0^{\mathbf{r}} N(\mathbf{r}')\,d\mathbf{r}' = \int_0^{\mathbf{r}} (f(\mathbf{r}')/\pi r'^2)\,d\mathbf{r}',$$

155 with $\frac{\partial^2}{\partial r \partial h}(C) = N(\mathbf{r}) = f(\mathbf{r})/\pi r^2$, and it obeys the conservation equation,

$$C(\mathbf{r}, t) = C(\mathbf{r} + \mathbf{G}\,dt, t + dt),$$

since floes with a finite size and thickness $\mathbf{r} = (r, h)$ are, by assumption, neither created nor destroyed
by thermodynamic growth and melting. Expanding the right hand side and rearranging in the limit

as $dt \to 0$ leads to the time rate of change of the cumulative number distribution,

$$\frac{\partial C(\mathbf{r}, t)}{\partial t} = -\mathbf{G} \cdot \nabla_\mathbf{r} C, \tag{3}$$

where $\nabla_\mathbf{r} = (\frac{\partial}{\partial r}, \frac{\partial}{\partial h})$ is the vector of partial derivatives in (size, thickness) space. Changes to the cumulative number distribution are due to the transfer of ice to larger or smaller sizes by thermodynamic growth and melting. We next make the assumption that thickness changes due to melting and freezing do not depend on the floe radius, and that horizontal size changes do not depend on the thickness, i.e., $\frac{\partial}{\partial h}(G_r) = \frac{\partial}{\partial r}(G_h) = 0$. The time evolution of the floe size distribution solely due to freezing and melting of existing floes is derived by taking derivatives with respect to both thickness and size of (3),

$$\begin{aligned}
\frac{\partial f(\mathbf{r})}{\partial t}\bigg|_{\text{melt/freeze}} &= -\pi r^2 \frac{\partial}{\partial r}\left(\frac{f(\mathbf{r})}{\pi r^2} G_r\right) - \frac{\partial f(\mathbf{r})}{\partial h} G_h, \\
&= -\nabla_\mathbf{r} \cdot (f(\mathbf{r})\mathbf{G}) + \frac{2}{r}f(\mathbf{r})G_r.
\end{aligned} \tag{4}$$

Without loss of generality, consider the interpretation of this equation for the case of freezing in which existing floes get thicker and larger. This implies that some of the area $f(\mathbf{r})$ now moves to larger ice classes, represented by the first term in (4). Note that the integral over all size classes and thickness of the first term vanishes, and therefore it does not describe ice area growth. The total ice area added or removed that belongs to floes of size r, $N(\mathbf{r})d/dt(\pi r^2)$, equal to $N(\mathbf{r})2\pi r G_r$, which is equal to the second term in (4).

Zhang et al. (2015) include the effects of melting and freezing on the FSD, in a way that depends on the lateral growth rate (our G_r), but without evaluating this rate in terms of thermodynamic forcing. Their formulation seems to lack the second term on the rhs of (4). The formulation presented here is for the joint FSTD, and therefore depends on both G_r and G_h. We further evaluate these rates below in terms of air-sea fluxes.

In addition to melting and freezing of existing floes we must also consider the rate of growth of pancake ice, $\dot{A}_p$, due to the flocculation of frazil crystals in patches of open water away from existing floes. Pancakes are assumed to be created by freezing at the smallest size and thickness accounted for in the model, with an effective radius r_p and thickness h_min. The full expression for the rate of change of the floe size and thickness distribution due to thermodynamics, $\mathcal{L}_T$, is therefore,

$$\mathcal{L}_T = -\nabla_\mathbf{r} \cdot (f(\mathbf{r})\mathbf{G}) + \frac{2}{r}f(\mathbf{r})G_r + \delta(r - r_{\text{min}})\delta(h - h_{\text{min}})\dot{A}_p. \tag{5}$$

The floe size and thickness change rate vector $\mathbf{G} = (G_r, G_h)$ is determined using the balance of heat fluxes at the ocean/ice/atmosphere interface. Note that our focus here is the impact of thermodynamic forcing on the FSTD: we are not modeling internal ice thermodynamics explicitly. In an application of the FSTD model, a full thermodynamic model of the ocean mixed layer and sea

6

ice would simulate the ice energy budget. Net heat flux in ocean regions adjacent to ice floes (which we refer to as lead regions) is assumed to affect the development of adjacent floes laterally and vertically, while cooling in open water away from existing floes may lead to pancake ice formation

195   (the model does not resolve frazil ice, nor arbitrarily small pancake ice). The lead region is defined as the annulus around each floe of width $r_{\overline{p}}r_{\text{lw}}$, and the division of ocean area into lead and open water areas is shown as the blue and white regions in Fig. 1, (see also Parkinson and Washington, 1979). The total lead area, A_{lead}, is approximated as,

$$A_{lead} = \min\left(\iint_{\mathbf{r}}\left(N(\mathbf{r})\pi(r+r_{\underline{\text{plw}}})^2 - N(\mathbf{r})\pi r^2\right)d\mathbf{r}, \phi\right)$$

200
$$= \min\left(\iint_{\mathbf{r}} f(\mathbf{r})\left(\frac{2r_p}{r}\frac{2r_{\text{lw}}}{r} + \frac{r_p^2}{r^2}\frac{r_{\text{lw}}^2}{r^2}\right)d\mathbf{r}, \phi\right),$$

where ϕ is the open water fraction, and the above integration is over the entire ranges of effective radius and thickness represented in the model. A net air-sea heat flux Q at the ocean surface is therefore partitioned into a lead heat flux $Q_{lead} = A_{lead}Q$ and an open water heat flux $Q_o = (\phi - A_{lead})Q$. If the water is at its freezing point, a cooling heat flux leads to freezing of pancakes of ice

205   of radius $r_{\overline{p}}$ and thickness $h_{\overline{p}}$ $r_{\min}$ and thickness $h_{\min}$, producing the area $\dot{A}_p$ of ice pancakes per unit time where there was formerly open water,

$$\dot{A}_p = \frac{Q_o}{\rho_0 L_f h_p}\frac{Q_o}{\rho_0 L_f h_{\min}}.$$

The lead region heat flux, Q_{lead}, is further partitioned into a part that leads to basal freezing or melting of existing ice floes, $Q_{l,b}$, and a component that leads to lateral freezing or melting along

210   perimeters of existing floes, $Q_{l,l}$. Multiple choices for this partitioning are possible, including a binary partition (Washington et al., 1976) with $Q_{l,b} = Q_{lead}$, $Q_{l,l} = 0$ or $Q_{l,l} = Q_{lead}$, $Q_{l,b} = 0$, a parameterization with a quadratic dependence on open water fraction $Q_{l,l} \propto A_{lead}^2$ (Parkinson and Washington, 1979), and diffusive and molecular-sublayer parameterizations based on the temperature of the surface waters (Steele, 1992; McPhee, 1992). While these parameterizations have been

215   tested in some detail (Harvey, 1990; Steele, 1992), sensitivity analyses in previous studies have fixed (either explicitly or implicitly) the floe size distribution, and the impact of this assumption on the results is unclear. We choose to simply assume that the lead heat flux is mixed uniformly over the exposed surface of a floe, partitioned according to the ratio of ice basal and lateral surface areas, where it contributes to ice growth or melt. The total fractional lateral surface area (that is, the area

220   of the vertical edges of ice floes, per unit ocean area) is

$$\iint_{\mathbf{r}} N(\mathbf{r})2\pi rh\, d\mathbf{r} = \iint_{\mathbf{r}} f(\mathbf{r})\frac{2h}{r}\, d\mathbf{r} = \overline{2h/r},$$

where N is the number distribution introduced above, $2\pi rh$ is the lateral area of one floe, and $\overline{2h/r}$ represents an average over all ice floes, weighted by the floe size and thickness distribution. The

7

above result depends on the model including an explicit joint FSTD, without which this estimate for
the lateral area would not be possible to obtain. The total basal ice surface area per unit ocean area is
the ice concentration, c. The partitioning of heat flux from the lead region between the ice base and
ice edges is therefore,

$$Q_{l,l} = Q_{lead}\left(1 + \frac{c}{\overline{2h/r}}\right)^{-1}; \quad Q_{l,b} = Q_{lead}\left(1 + \frac{\overline{2h/r}}{c}\right)^{-1}.$$

The rate of change of ice thickness can be found using a model of ice thermodynamics, given the
above derived open-water air-sea flux contribution $Q_{l,b}$ to the heat budget at the ice base. For exam-
ple, ignoring ice heat capacity, ice thickness changes due to melting and freezing are related to the
net heat flux into the ice from the surface above, Q_{surf} (defined negative upward), and from below
(where negative flux means ocean cooling),

$$\rho_i L_f G_h = -(Q_{l,b} + Q_{\mathrm{surf}}). \tag{6}$$

The rate of change of the lateral floe size is calculated from the corresponding contribution of the
air-sea heat flux from the lead region $Q_{l,l}$,

$$\rho_i L_f G_r = -Q_{l,l}. \tag{7}$$

The above equations can now be used to express the thermodynamic floe growth rate vector, ~~$\mathbf{G} = (\dot{r}, \dot{h})$~~ $\mathbf{G} = (G_r, G_h)$.

2.2 Mechanical interactions

Wind and ocean currents can drive individual floe collisions, and therefore merge them together.
When one floe overrides another while remaining intact, the interaction is referred to as rafting. If
the ice at the point of contact disintegrates into a rubble pile, forming a 'sail' and a 'keel', and the two
floes consolidate, the interaction is referred to as ridging. To describe these processes, open water in
the floe size and thickness distribution $f(\mathbf{r})$ is represented by a delta function at $\mathbf{r} = 0$, multiplied
by the area fraction of open water. The dynamics of open water formation by ice flows may then
be derived by taking integrals over the prognostic equation (2) that include or exclude $\mathbf{r} = 0$ (a list
of the variables used to describe the FSTD response to floe collisions is provided in Table 3). ~~Since
the integral of $f(\mathbf{r})$~~ The integral of $f(\mathbf{r})$ over all floe sizes ~~including zero~~ and thicknesses, including
open water, is equal to ~~1~~ one. Therefore, ignoring thermodynamic and wave effects, ~~and including
the contribution of open water by taking the integral of~~ we integrate (2) over a range of floe sizes

that includes a vanishingly small interval of sizes around $\mathbf{r} = (r, h) = \mathbf{0}$,

$$\int_{\mathbf{0}^-} \mathcal{L}_M(\mathbf{r})\, d\mathbf{r} \equiv \lim_{|(\epsilon_1,\epsilon_2)| \to 0} \int_{-\epsilon_1}^{\infty} \int_{-\epsilon_2}^{\infty} \mathcal{L}_M(r,h)\, dr\, dh,$$

$$= \int_{\mathbf{0}^-} \left[\frac{\partial f(\mathbf{r})}{\partial t} + \nabla \cdot (f(\mathbf{r})\,\mathbf{u})\right] d\mathbf{r},$$

$$= \frac{\partial 1}{\partial t} + \nabla \cdot (1\,\mathbf{u}) = \nabla \cdot \mathbf{u}. \tag{8}$$

255 ~~Next, as the~~ The integral of $f(\mathbf{r})$ over all floe sizes and thicknesses, but excluding open water ($\mathbf{r}$ = 0), is equal to the ice concentration~~c, integrating~~, c. Integrating (2) ~~again but~~ as before but now excluding $\mathbf{r} = \mathbf{0}$,

$$\int_{\mathbf{0}^+} \mathcal{L}_M(\mathbf{r})\, d\mathbf{r} \equiv \lim_{|(\epsilon_1,\epsilon_2)| \to 0} \int_{\epsilon_1}^{\infty} \int_{\epsilon_2}^{\infty} \mathcal{L}_M(r,h)\, dr\, dh,$$

$$= \int_{\mathbf{0}^+} \left[\frac{\partial f(\mathbf{r})}{\partial t} + \nabla \cdot (f(\mathbf{r})\,\mathbf{u})\right] d\mathbf{r},$$

260
$$= \frac{\partial c}{\partial t} + \mathbf{u} \cdot \nabla c + c(\nabla \cdot \mathbf{u}) \equiv \frac{D_M c}{Dt}. \tag{9}$$

The above definition of operator D_M/Dt implies that $D_M(1)/Dt = \nabla \cdot \mathbf{u}$. The subscript M indicates that this operator represents concentration changes due to mechanical interactions only. $D_M c/Dt$ is equal to the total sea-ice area which is eliminated due to the collisions of floes per unit time. Subtracting (8) from (9),

265
$$\int_{\mathbf{0}^-}^{\mathbf{0}^+} \mathcal{L}_M(\mathbf{r})\, d\mathbf{r} = \nabla \cdot \mathbf{u} - \frac{D_M c}{Dt}.$$

This result implies that $\mathcal{L}_M(\mathbf{r})$ has a $\delta(\mathbf{r})$ component due to open water creation in floe collisions, or the integral on the infinitesimally small range near zero size would have vanished. ~~In addition, equation~~ Note that the function $\delta(\mathbf{r})$ is the two-dimensional delta function: $\delta(\mathbf{r}) = \delta([r,h]) \equiv \delta(r)\delta(h)$. Equation (9) suggests that there should be another term in $\mathcal{L}_M(\mathbf{r})$ that, when integrated over all sizes

270 leads to $D_M c/Dt$. This suggests the following form,

$$\mathcal{L}_M = (\nabla \cdot \mathbf{u})\delta(\mathbf{r}) + \frac{D_M c}{Dt}\left[\mathrm{L}_c(\mathbf{r}) - \delta(\mathbf{r})\right], \tag{10}$$

where $\mathrm{L}_c(\mathbf{r})$ is yet unspecified except that its integral over all sizes is one, and it is non-singular at $||\mathbf{r}|| = 0$,

$$\int_{\mathbf{0}^+} \mathrm{L}_c(\mathbf{r})\, d\mathbf{r} = \int_{\mathbf{0}^-} \mathrm{L}_c(\mathbf{r})\, d\mathbf{r} = 1. \tag{11}$$

275 The factor $\mathrm{L}_c(\mathbf{r})$ quantifies the relative fraction of the total concentration lost due to collisions at each floe size. The terms in (10) that are proportional to $\delta(\mathbf{r})$ represent together the formation of

9

open water due to collisions driven by divergent ice motions. The remaining term represents the rearrangement of ice area among floe classes. It remains to derive expressions for the rate of open water formation due to collisions $D_M c/Dt$, and the rearrangement of the floe size and thickness distribution in response to a unit amount of open water formation due to collisions, $L_c(\mathbf{r})$.

Thorndike et al. (1975) described the rate of mechanical interactions as depending on the divergence, convergence and shear of the ice flow, weighted by the relative size of the invariants of the ice strain rate tensor $\dot{\boldsymbol{\epsilon}}$,

$$\dot{\epsilon}_{ij} = \frac{1}{2}\left(\frac{\partial u_i}{\partial x_j} + \frac{\partial u_j}{\partial x_i}\right). \tag{12}$$

Defining the deviatoric strain tensor, $\dot{\epsilon}'_{ij} = \dot{\epsilon}_{ij} - \delta_{ij}\nabla\cdot\mathbf{u}/2$, equal to the divergence-free part of $\dot{\epsilon}_{ij}$, two relevant invariants may be written as $\mathbf{E} = (\epsilon_I, \epsilon_{II}) = (\nabla\cdot\mathbf{u}, 2|-\dot{\boldsymbol{\epsilon}}'|^{1/2})$. The first invariant is the flow divergence and the second is calculated from the determinant of the deviatoric strain rate tensor, and is equal to the maximal shear strain rate. Given these definitions, we parameterize the rate of ice area loss due to collisions as,

$$\frac{D_M c}{Dt} = \frac{1}{2}\left(\epsilon_I - ||\mathbf{E}||\right) \leq 0, \tag{13}$$

which allows us to write the mechanical interaction term in the FSTD equation as,

$$\mathcal{L}_M = \delta(\mathbf{r})\epsilon_I + \frac{1}{2}\left(||\mathbf{E}|| - \epsilon_I\right)\left[\delta(\mathbf{r}) - L_c\right]. \tag{14}$$

This formulation is exactly equivalent to that of Thorndike et al. (1975), see appendix for details. In the case of ice flow characterized by pure divergence, $\mathbf{E} = (\nabla\cdot\mathbf{u}, 0)$ and $\nabla\cdot\mathbf{u} > 0$, the mechanical interactions are represented as a delta function at $\mathbf{r} = 0$, representing only the formation of open water by divergent ice flow. In pure convergence, $\mathbf{E} = (\nabla\cdot\mathbf{u}, 0)$ and $\nabla\cdot\mathbf{u} < 0$, and mechanical interactions create open water through collisions and $\mathcal{L}_M(\mathbf{r}) = |\nabla\cdot\mathbf{u}|L_c(\mathbf{r})$. When the ice flow is characterized by shear motions, $||\mathbf{E}|| = \epsilon_{II}$, and collisions still occur due to the differential motion of neighboring floes, which forms open water at a rate of $D_M c/Dt = \epsilon_{II}/2$ per second. Other choices of $D_M c/Dt$ could satisfy (10), but the Thorndike parameterization meets the intuitive requirements that in pure divergence no collisions occur, while in pure convergence they do, and in pure shear collisions occur such that the rate of open water formation per unit strain is reduced relative to the case of pure convergence.

The effects of mechanical interactions on the FSD are represented by Zhang et al. (2015) similarly to (10), with the rate of area loss (our $D_M c/Dt$) taken from Hibler III (1980), and assuming that all floes of different sizes have same ITD. In our joint FSTD formulation, the mechanical interactions are represented for floes characterized by both specific thickness and specific size. Here, interactions between floes are treated as binary collisions, and our model does not consider multiple simultaneous collisions in a single time step. Such multiple collisions lead to clustering, which is relevant for granular media undergoing deformation (Shen and Sankaran, 2004), with sea ice being

a possible example. However, Herman (2013) demonstrated in numerical simulations that floes may also aggregate into clusters via a sequence of binary interactions between pairs of floes.

The rearrangement of floe area in response to a unit amount of open water formation, $L_c(\mathbf{r})$, is represented using a collision kernel $K(\mathbf{r}_1, \mathbf{r}_2; \mathbf{r})$. Let $K(\mathbf{r}_1, \mathbf{r}_2; \mathbf{r}) \, d\mathbf{r}_1 \, d\mathbf{r}_2 \, d\mathbf{r}$ be equal to the number of collisions per unit time between floes in the range $(\mathbf{r}_1, \mathbf{r}_1 + d\mathbf{r}_1)$ and floes in the range $(\mathbf{r}_2, \mathbf{r}_2 + d\mathbf{r}_2)$, that form floes in the range $(\mathbf{r}, \mathbf{r} + d\mathbf{r})$, per unit area of open water formation. In general, the floe number distribution subject to mechanical combination of floes evolves according to

$$\frac{\partial N(\mathbf{r})}{\partial t} = \int\limits_{\mathbf{r}_1} \int\limits_{\mathbf{r}_2} \left[\frac{1}{2} N(\mathbf{r}_1) N(\mathbf{r}_2) K(\mathbf{r}_1, \mathbf{r}_2; \mathbf{r}) \right.$$
$$\left. - N(\mathbf{r}) N(\mathbf{r}_2) K(\mathbf{r}, \mathbf{r}_2; \mathbf{r}_1) \right] d\mathbf{r}_1 \, d\mathbf{r}_2, \tag{15}$$

where the ~~integrals are over all resolved floe sizes~~ notation $\int\limits_{\mathbf{r}} d\mathbf{r}$ is taken to mean an integral over all floe sizes and thicknesses resolved by the model. The factor of 1/2 prevents double-counting: since K is symmetric with respect to its first two arguments, each interaction pair $(\mathbf{r}_1, \mathbf{r}_2)$ is counted twice in the integral in (15). This represents the rate of change in the number of floes of size $\mathbf{r}_3$ due to mechanical interactions. In reality, some floe collisions may lead to a rebound and erosion of floe edges rather than to a merging of the floes, yet we do not account for such a process. The first term on the right-hand side of (15) represents the increase in floe number at size $\mathbf{r}$ due to collisions between floes of other sizes, and the second term represents the loss in floe number at size $\mathbf{r}$ due to combination of floes of size $\mathbf{r}$ with other floes. Equation (15) is a generalization of the Smoluchowski coagulation equation that has been previously used to model the sea-ice thickness distribution (Godlovitch et al., 2011). If we multiply equation (15) by the area of a floe of size $\mathbf{r}$, we obtain the rate of change of the fractional area covered by floes of size $\mathbf{r}$ due to mechanical interactions, which is nothing but the definition of $\mathcal{L}_M(\mathbf{r})$,

$$\frac{\partial f(\mathbf{r})}{\partial t} = (\pi r^2) \frac{\partial N(\mathbf{r})}{\partial t} = \mathcal{L}_M(\mathbf{r}); \; (r \neq 0). \tag{16}$$

We already concluded above that away from $\mathbf{r} = 0$ we have $\mathcal{L}_M(\mathbf{r}) = L_c(\mathbf{r})$. Therefore the above eqn gives,

$$L_c(\mathbf{r}) = (\pi r^2) \frac{\partial N(\mathbf{r})}{\partial t}, \tag{17}$$

where $\partial N / \partial t$ is taken from (15). We represent the kernel $K(\mathbf{r}_1, \mathbf{r}_2, \mathbf{r})$ as the product of two factors. The first is the probability of collision via ridging or rafting of two floes of size $\mathbf{r}_1$ and $\mathbf{r}_2$, termed $P_{coll}(\mathbf{r}_1, \mathbf{r}_2)$ where the subscript "coll" is either "ridge" or "raft", and the probabilities are to be defined more specifically shortly.

The second factor is a delta function, $\delta(\mathbf{r} - R(\mathbf{r}_1, \mathbf{r}_2))$, that limits the pairs of collision partners to only those that form a floe of size $\mathbf{r} = R(\mathbf{r}_1, \mathbf{r}_2)$, specified below, and whose area is smaller than

11

the area of the two colliding floes combined. Noting again that the number distribution and area distribution are related through $N(\mathbf{r}) = \pi r^2 f(\mathbf{r})$, we combine (17) and (15) to find,

$$L_c(\mathbf{r}) = L_c^* \iint\limits_{\mathbf{r}_1, \mathbf{r}_2} \left[\frac{1}{2} \frac{r^2}{\pi r_1^2 r_2^2} f(\mathbf{r}_1) f(\mathbf{r}_2) P_{coll}(\mathbf{r}_1, \mathbf{r}_2) \delta(\mathbf{r} - R(\mathbf{r}_1, \mathbf{r}_2)) \right.$$

$$\left. - \frac{1}{\pi r_2^2} f(\mathbf{r}) f(\mathbf{r}_2) P_{coll}(\mathbf{r}, \mathbf{r}_2) \delta(\mathbf{r}_1 - R(\mathbf{r}, \mathbf{r}_2)) \right] d\mathbf{r}_1 d\mathbf{r}_2. \tag{18}$$

The coefficient L_c^* is a normalization constant ensuring that the integral over $L_c(\mathbf{r})$ is one (11). In the discretized version of equation (18), two floe classes of discrete size $\mathbf{r}_1^d$ and $\mathbf{r}_2^d$ which combine to form floes of discrete size $\mathbf{r}^d$ do not necessarily satisfy $\pi(r_1^d)^2 h_1^d + \pi(r_2^d)^2 h_2^d = \pi(r^d)^2 h^d$. Ice volume conservation that is independent of the discretization is achieved by determining the newly formed area of the new floes, in each time step, using the constraint that volume must be conserved,

$$\Delta f(\mathbf{r}_1^d) h_1^d + \Delta f(\mathbf{r}_2^d) h_2^d = -\Delta f(\mathbf{r}^d) h^d,$$

where $\Delta f(\mathbf{r})$ is the area change at size $\mathbf{r}$ in a single timestep due to the mechanical interaction considered here. Thus the total volume lost by floes at size $\mathbf{r}_1^d$ and $\mathbf{r}_2^d$ (lhs) is equal to the corresponding volume gained at size $\mathbf{r}_3^d$ (rhs).

2.2.1 Probability of collision

We choose the functions $P_{coll}(\mathbf{r}_1, \mathbf{r}_2)$ to be proportional to the probability that two floes of size $\mathbf{r}_1$ and $\mathbf{r}_2$ will overlap if placed randomly in the domain, and they are calculated in a similar manner for both mechanical processes (rafting or ridging). We consider such an overlap as an indication that mechanical interaction has occurred. The area of each floe that may be deformed due to mechanical interactions is restricted to a small region near the edge of the floe, represented in our model by a narrow annulus~~of width $\delta = \delta_{ridge}$ or $\delta = \delta_{raft}$~~, which we term a "contact zone", of width $\delta_{cz} = \delta_{ridge}$ or $\delta_{cz} = \delta_{raft}$ at the floe edge, which depends on the floe size and the interaction type~~. We term these annuli the "contact zones" of the floes , with the interiors being the~~; we also term the interiors of floes "cores" (Fig. 1). The area of a single floe of size s is therefore broken down as,

$$\pi s^2 = A_{core}(s) + A_{cz}(s) = \pi(s - \delta_{cz})^2 + \pi(2\delta_{cz} s - \delta_{cz}^2).$$

The above defined probability of collision between floes of size r_1 and r_2 is proportional to the product of contact zone areas divided by the open ocean area, A, not including the core areas,

$$P_{coll}(\mathbf{r}_1, \mathbf{r}_2) \propto \frac{A_{cz}(r_1) A_{cz}(r_2)}{(A - A_{core}(r_1) - A_{core}(r_2))^2}.$$

The above probability that two floes will collide is based on geometric constraints. However, the rate of collisions depends also on the ice strain rate tensor $\dot{\boldsymbol{\epsilon}}$ as explained above, and this tensor depends on external forcings such as the strength of the prevailing winds and currents (Shen et al., 1987; Herman, 2011, 2013; Bennetts and W but the determination of that relationship is not a focus of the FSTD model presented here.

Data of the morphology and width distribution of ridges and rafts as a function of the size of the combining ice floes are scarce, though there are indications that rafts can be substantially larger than ridges (Hopkins et al., 1999). We crudely define the width of the contact zone in ridging to be 5 meters, or the size of the smaller of the two combining floes, whichever is smaller,

$$\delta_{ridge}(r_1, r_2) = \min(5 \text{ m}, r_1, r_2).$$

For rafting, we assume a larger portion of the smaller floe may be uplifted, up to 10 meters,

$$\delta_{raft}(r_1, r_2) = \min(10 \text{ m}, r_1, r_2).$$

Both choices lead to larger ridges and rafts as the size of the interacting floes increases. Given observations of these processes one can refine the above choices, to which our model is not overly sensitive. Finally, we assume that ridging occurs for floes thicker than 0.3 m, and rafting occurs when both floes are thinner than 0.3 m, consistent with the study of Parmerter (1975), with a smooth transition between the two regimes implemented by a coefficient $\gamma(h)$ which tends to one for thicknesses that are prone to rafting and to zero for ridging,

$$K(\mathbf{r}_1, \mathbf{r}_2; \mathbf{r}) = \gamma(h_1)\gamma(h_2)\mathrm{P}_{raft}(\mathbf{r}_1, \mathbf{r}_2)\delta(\mathbf{r} - \mathrm{R}_{raft}(\mathbf{r}_1, \mathbf{r}_2))$$
$$+ (1 - \gamma(h_1)\gamma(h_2))\mathrm{P}_{ridge}(\mathbf{r}_1, \mathbf{r}_2)\delta(\mathbf{r} - \mathrm{R}_{ridge}(\mathbf{r}_1, \mathbf{r}_2)),$$
$$\gamma(h) = \frac{1}{2} - \frac{1}{2}\tanh\left[(h - 0.3)/0.05\right].$$

2.2.2 New floe size

The ice area lost in an interaction is different for rafting and ridging. In rafting, the entire contact zone is replaced by ice whose thickness is the sum of that of the original floes. In ridging, the contact zone is increased in thickness by a factor of 5, compressing its area by a factor of 1/5 (Parmerter and Coon, 1972). Given that our model assumes each floe has a uniform thickness, we treat floes formed by ridging or rafting to be of uniform thickness, chosen to conserve volume. This choice eliminates the need for keeping track of sea-ice ~~morpology, and as these features occur at the interior of new floes , they are of lesser importance to further mechanical interactions the we assume to occur at floe boundaries.~~ morphology. Observations (Collins et al., 2015; Kohout et al., 2015) have indicated that floes may break up along ridges, in which case equation (18) may be used to provide information about the ridge density. This is a potential future extension of the present work.

Assuming without loss of generality that $r_1 \leq r_2$, the area of the newly formed floes is therefore given by the sum of the areas minus the area lost to either ridging or rafting. We then divide this area by π and take the square root to find the size of the newly formed floes. The thickness of the formed

13

floe is calculated from volume conservation. We therefore have,

$$[r,h] = \mathbf{R}([r_1,h_1],[r_2,h_2])_{raft}$$

$$= \left(\sqrt{r_1^2 + r_2^2 - \frac{1}{2} A_{cz,raft}(r_1)/\pi}, \frac{V(\mathbf{r_1}) + V(\mathbf{r_2})}{\pi r^2} \right),$$

$$[r,h] = \mathbf{R}([r_1,h_1],[r_2,h_2])_{ridge}$$

$$= \left(\sqrt{r_1^2 + r_2^2 - \frac{4}{5} A_{cz,ridge}(r_1)/\pi}, \frac{V(\mathbf{r_1}) + V(\mathbf{r_2})}{\pi r^2} \right),$$

where $V(\mathbf{r}) = V([r,h]) = h\pi r^2$ is the volume of an ice floe.

2.3 Swell fracture

Sea surface height variations due to surface ocean waves strain and possibly break sea-ice floes into smaller floes of varying sizes. Since this process does not create or destroy sea-ice area, ~~wave-breaking~~ the response of the FSTD to fracture of sea ice by waves obeys the conservation law,

$$\iint\limits_{\mathbf{r}} \mathcal{L}_W(\mathbf{r})\, d\mathbf{r} = 0,$$

where $\mathcal{L}_W(\mathbf{r})$ is the time rate of change of floes of size and thickness $\mathbf{r} = (r,h)$ due to ~~wave fracture~~ fracture of ice by surface waves in (2), and the integral is over all sizes and thicknesses (a list of the variables used to describe the response of the FSTD to ~~wave fracture~~ ice fracture by waves is provided in Table 4). Suppose that an area of floes $\Omega(\mathbf{r},t)\,d\mathbf{r}$ with sizes between $\mathbf{r}$ and $\mathbf{r} + d\mathbf{r}$ is fractured per unit time. Let new floes resulting from this process have the floe size distribution $F(\mathbf{r},\mathbf{s})\,d\mathbf{s}$, equal to the fraction of $\Omega(\mathbf{r},t)$ that becomes floes with size between $\mathbf{s}$ and $\mathbf{s} + d\mathbf{s}$. The rate of change of area of floes of size $\mathbf{r}$ due to ~~wave-breaking~~ fracture by ocean surface waves is then,

$$\mathcal{L}_W(\mathbf{r}) = -\Omega(\mathbf{r},t) + \int\limits_{\mathbf{s}} \Omega(\mathbf{s},t)F(\mathbf{s},\mathbf{r})\,d\mathbf{s}. \tag{19}$$

The first term is the loss of fractional area of size $\mathbf{r}$ that is fractured per unit time, and the second is the increase in the area occupied by floes of size $\mathbf{r}$ due to the fracture of floes of larger sizes.

Kohout and Meylan (2008) modeled floes as long floating elastic plates, and showed ocean surface waves to be attenuated exponentially as a function of the number, Λ, of ice floes the waves encounter as they propagate into an ice pack. Wave energy therefore decays as $\exp(-\alpha\Lambda)$, where the attenuation coefficient is $\alpha(T,\bar{h})$, T is the wave period, and $\bar{h}$ the mean ice thickness. We approximate the number of floes per unit distance as $c(2\bar{r})^{-1}$, where c is the ice concentration and $\bar{r}$ the average effective radius. The attenuation distance, W, is then given by the inverse of the attenuation per floe times the number of floes per unit distance $W(T,\bar{h}) = 2\bar{r}(c\alpha)^{-1}$. We approximate this attenuation by fitting the attenuation coefficient $\alpha(T,\bar{h})$ calculated by Kohout and Meylan (2008)

14

(their Fig. 6) to a quadratic function of the period and mean thickness (Fig. 2). Kohout and Meylan
(2008) only report an attenuation coefficient for wave periods longer than 6 seconds and thicknesses
less than 3 meters (red box in Fig. 2), so we extrapolate to shorter periods and higher thicknesses
using this fit when necessary. ~~Our formulation of the effects of wave fracture depends on their wavelengths rather than periods, and we use the~~ Scattering models may under-predict attenuation rates (Williams et al., 2012) , which may allow for longer penetration of waves into the MIZ than is physically realistic. Updated models of the wave attenuation (Bennetts and Squire, 2012) suggest different attenuation coefficients as function of wave period and ice thickness. We tested our model with the Bennetts and Squire (2012) attenuation coefficient, and show in the supplement, (Sec. S1.4), that our FSTD model can be sensitive to the choice of attenuation model. Future applications of this FSTD model should therefore carefully consider the wave attenuation formulation, based on both model estimates and observations (e.g., Meylan et al., 2014) .

We convert the attenuation coefficients, reported as a function of wave period, to a function of wavelength using the deep-water surface gravity wave dispersion relation, $\lambda = gT^2/2\pi$ ~~to convert between the two~~. Let the width of the domain to which the FSTD model is applied be D (e.g., the width of a GCM grid cell which borders on open water). The fraction of the grid cell area in which waves of wavelength λ may break floes is therefore estimated as $\min(W(\lambda, \overline{h})/D, 1)$. The duration $\tau(\lambda)$ over which breaking occurs is approximated as the domain width divided by the group velocity for surface gravity waves,

$$\tau(\lambda) = \frac{D}{c_g(\lambda)} = 2D\sqrt{\frac{2\pi}{g\lambda}}.$$

Observations of wave propagation in ice (Collins et al., 2015) have suggested that the propagation speed of fracture in ice may be slower than the group velocity of surface waves. With more data, the above choice for $\tau(\lambda)$ may be re-evaluated.

We assume floes flex with the sea surface height, and for a monochromatic and unidirectional wave field of wavelength λ and amplitude a, the maximal strain of a floe of thickness h occurs at the crest and trough of the wave, with magnitude $\epsilon_{max} = a\,h2\pi^2/\lambda^2$ (Dumont et al., 2011, p. 4). If the maximum strain exceeds an empirically defined value ϵ_{crit}, the floe will break, and since the maximum strain occurs between the trough and crest of the wave, the fracture leads to floes of size $\lambda/2$. If the wavelength is larger than the floe radius, the floe ~~will not be fractured.~~ is not fractured. This specification of the minimum floe size that may be fractured by a wave of wavelength λ is somewhat arbitrary, and based on the heuristic assumption that smaller floes float without being significantly strained by the waves. A better choice of this minimum floe size requires further observations and modeling.

~~The~~ Our approach is to determine the floe size distribution caused by the fracture of ice by surface waves, $F(\mathbf{s}, \mathbf{r})$, based on the wave spectrum. Williams et al. (2013a) used a Rayleigh distribution for the strain spectrum to predict breaking of floes, however this does not determine the floe sizes

15

470 produced by the breaking. The central assumption that we will make in determining the expression for $F(\mathbf{s}, \mathbf{r})$ is that individual wave components act separately on floes. The amplitude of waves with wavelengths in the range λ to $\lambda + d\lambda$ is approximated ~~as $a(\lambda) \approx \sqrt{S(\lambda) d\lambda}$, where $S(\lambda)$ is the normalized wave energy spectrum (in units of m, see Bouws et al., 1998, p. 11)~~ following $a(\lambda) \approx \sqrt{2S(\lambda) d\lambda}$ (see Bouws et al. (1998), p.11 and Meylan et al. (2014), eq. 2). The spectrum $S(\lambda) d\lambda$ ~~represents~~

475 ~~the total wave energy~~ is equal to half the mean amplitude squared of waves belonging to waves with wavelengths between λ and $\lambda + d\lambda$, equal to the total wave energy in this wavelength band normalized by ρg. The range $d\lambda$ corresponds to the sampling resolution of Fourier components of the wave record (Bouws et al., 1998).

Since many wavelengths can fracture a floe of a given effective radius r, information about the
480 likelihood distribution of wave ~~heights~~ amplitudes $P_{wa}(a) da$, the probability of a wave amplitude lying in the range a to $a + da$, is used to complete the formulation. Observations of wave amplitudes (see Michel, 1968, p. 19) show ~~wave heights~~ them to be Rayleigh distributed,

$$P_{wa}(a) = \frac{2a}{H_s^2} \frac{8a}{H_s^2} \exp\left(\underline{-a}\, {-}8a^2 / H_s^2\right).$$

The probability $P_f(\mathbf{r}, \lambda)$ that a floe of size $\mathbf{r}$ fractures due to a wave of wavelength λ is therefore
485 chosen as,

$$P_f(\mathbf{r}, \lambda) = \begin{cases} A^{-1} P_{wa}(a(\lambda)) & \text{if } \epsilon_{crit} > \epsilon_{max}(\lambda, \mathbf{r}) \text{ and } \lambda < r, \\ 0 & \text{otherwise.} \end{cases} \tag{20}$$

The normalization by $A(\mathbf{r}) = \int P_{wa}(a(\lambda)) \theta(\epsilon_{crit}(\lambda, \mathbf{r}) - \epsilon_{max}) \theta(r - \lambda) d\lambda$, where $\theta(x)$ is the Heaviside step function, assures that the integral of P_f over all wavelengths is equal to 1 if the floes of size $\mathbf{r}$ will break. We note again that the distribution of both floe size and thicknesses plays a
490 critical role in determining the fracture of ice by waves, underlying the need to use the coupled FSTD for representing the effects of ice fracture due to surface waves. In the case of monochromatic swell waves, which are not described by a Rayleigh distribution, the only contribution of $P_{wa}(a(\lambda))$ to $P_f(\mathbf{r}, \lambda)$ is at the wavelength of the swell, as the wave amplitude $a(\lambda)$ is zero for all other wavelengths. Since the wavelength required to form a floe of size r is $\lambda = 2r$, the size distribution
495 of floes resulting from the fracture of floes of size $\mathbf{s}$, $F(\mathbf{s}, \mathbf{r})$, is equal to

$$F(\mathbf{s}, \mathbf{r}) = F\left((s, h_s), (r, h_r)\right) = P_f((s, h_s), 2r) \delta(h_s - h_r),$$

where the first term is the probability that a floe of size (s, h_s) will be fractured by a wave of wavelength $\lambda = 2r$, and the delta function represents the fact that ice that is fractured does not change its thickness. The function $\Omega(\mathbf{r}, t) d\mathbf{r}$, which is the fractional area fractured per unit time that
500 belongs to floes of size between $\mathbf{r}$ and $\mathbf{r} + d\mathbf{r}$, can now be written,

$$\Omega(\mathbf{r}, t) = \int \frac{1}{\tau(\lambda)} \min\left(\frac{W(\lambda, \overline{h})}{D}, 1\right) P_f(\mathbf{r}, \lambda) d\lambda.$$

16

The first two factors under the integral sign represent the rate at which waves enter the domain, and the fractional area of the domain that they reach. This is multiplied by the probability that such waves are observed and will fracture floes of size **r**, which depends on the wave spectrum in the marginal ice zone. Waves that attenuate rapidly are less capable of breaking a large area of floes.

The effects of ~~wave fracture~~ the fracture of ice by waves on the FSD is represented by Zhang et al. (2015) based on an expression similar to (19), assuming that only floes with horizontal size larger than a specified threshold break, that a fractured floe is equally likely to form any smaller size within a specified range, and that all floes in a given size class have the same ITD. In the representation in the present paper of the effects of ~~wave fracture~~ ice fracture by waves on the joint FSTD, the wave spectrum plays a central role in determining the resulting floe sizes, as well as the propagation distance over which ocean waves are attenuated by the ice field. Information about the specific thickness of individual floe sizes informs the strain rate failure criterion and therefore determines which floes will be fractured.

3 Model results

To demonstrate and understand the model's response to a variety of forcing scenarios, we first examine its response over a single time step in three runs with idealized forcing fields. Each of these scenarios applies one of the following forcing fields: a net surface cooling $Q = -100\,\mathrm{W\,m^{-2}}$ which induces ice growth, a rate of ice flow convergence of $\nabla \cdot \mathbf{u} = -5 \times 10^{-9}\,\mathrm{s^{-1}}$ which induces floe collisions, and a surface gravity wave field of a single wavelength $\lambda = 56\,\mathrm{m}$ and amplitude of 1 m, leading to ~~wave~~ ice fracture. The model is initialized with a size and thickness distribution composed of two Gaussian peaks (Fig. 3a). The first (referred to as size I below) has a mean size of 90 m and a mean thickness of 0.25 m. Ice at this size and thickness is susceptible to ~~swell fracture~~ fracture by surface waves and rafting. The second peak (size II) has a mean size of 15 m and a mean thickness 1.5 m. Ice at this size and thickness tends to ridge rather than raft, and is not susceptible to ~~wave~~ fracture given our specified wave field. This second point is important, as it demonstrates a possible scenario in which knowledge of the ITD and FSD, ~~seperately~~separately, would not be sufficient to evolve the FSTD, as some floes, independent of their thickness, will not fracture. The initial sea-ice concentration is 75%. The domain width is $D = 10$ km, and the width of the lead region is set to be ~~$r_p = 0.5$~~ $r_{\mathrm{lw}} = r_{\mathrm{min}} = 0.5$ m, the smallest floe size resolved in this model. The critical strain amplitude for flexural failure, ϵ_{crit}, is set to 3×10^{-5} in line with other studies (Kohout and Meylan, 2008; Dumont et al., 2011). Williams et al. (2013a) formulated a more complex expression for the critical failure limit, and this was found to have a significant effect on wave fracturing (Williams et al., 2013b). We examine the model sensitivity to some of the main parameters used in these model simulations in the supplement (Sec. S1).

17

When two floes of size r and s combine due to rafting or riding interactions, they form a new floe with effective radius $r' > \max(r, s)$. For an arbitrary floe size discretization into size bins, this new size may not lie within a bin representing a size larger than those of the two interacting floes. As a result, interacting floes may accumulate at a single bin size rather than move into bins representing larger sizes. The minimum bin resolution necessary to avoid this problem is set by the interaction of two floes that are the same size r, with r smaller than the ridge width δ_{ridge}. When two such small floes interact via ridging in our model, one of them becomes 5 times thicker and its area is reduced by a factor of 5. They therefore form a floe of size $\sqrt{6/5}r$. We select a variable discretization, with $r_{n+1} = \sqrt{6/5}r_n$, with ~~26~~ 64 floe sizes between 0.5 and 156 meters. There are 14 thickness categories, 13 of which are equally spaced between 0.1 m to 2.5 m. To conserve volume when thick floes combine or grow due to freezing, the 14th thickness category incorporates all thicknesses greater than 2.5 m. We examine the numerical convergence of the model in the supplement (Sec. S2) finding that increasing this resolution does not significantly alter the numerical results.

The difference between the model state after a single one-hour time step and the model initial conditions is shown in Figs. 3b-d. Cooling leads to growth in both thickness and size (Fig. 3b) with the impact of lateral growth being less visible than the change in thickness. The shift in thickness is seen by the negative tendency (blue shading) for thicknesses smaller than the maximum of the initial distribution, and positive tendency at sizes larger than the initial maximum (red shading). These tendencies correspond to the shifting of floes from thinner to thicker floes due to the freezing. The shift in horizontal size is less apparent in the figure, due to the separation of scales between size and thickness: lateral growth rates are comparable to vertical growth rates (1 cm/day), but given that there is more than an order of magnitude difference between the floe size and thickness, the size change corresponds to a smaller relative change than the thicknesses change. The size response would be more apparent for smaller initial floe sizes not included in this idealized model experiment.

Mechanical interactions (Fig. 3c) lead to growth at three distinct clusters of size and thickness. The first, due to the self-interaction (rafting) of floes of size I, is shown as a positive tendency at a floe size of 123 m and thickness of 0.35 m. This cluster would not be resolved in a model that represented the ice thickness distribution only. The second cluster is due to a ridging interaction between floes of size I and II, leading to new floes of around 90 m size and 0.5 meters thickness. The third, due to self-interaction (ridging) between floes of size II, leads to a positive tendency at floe sizes around 17 meters and thickness around 1.7 meters. Both the second and third clusters of floes would not be resolved in a model that represents the floe size distribution only, showing again the importance of representing the joint FSTD.

Swell fracture (Fig. 3d) leads to the fracturing of many of the floes of size I, shown as a negative tendency at the eliminated size class. Floes of size II are not affected because they are smaller than twice the wavelength of the specified surface gravity wave field. Since the specified wave field is monochromatic, the area of floes of size I that are broken is shown as a positive tendency at a floe

18

size equal to half of the wavelength of the surface gravity wave, $\lambda/2 = 28$ m. Ice thickness does not change ~~during wave fracture~~<u>when the ice is fractured</u>.

575   Next, two one-month simulations are performed using the same initial distribution to show the behavior of the model forced by two different fixed strain rate scenarios (Fig. 4). The first (Fig. 4a,b) simulates convergence of fixed magnitude ($\epsilon_I = -10^{-7}, \epsilon_{II} = 0$) s^{-1}, and the second (Fig. 4c,d) simulates shear of fixed magnitude ($\epsilon_I = 0, \epsilon_{II} = 10^{-7}$) s^{-1}. When there is no convergence, the rate of open water formation due to collisions (13) is 0.5×10^{-7} s^{-1}, equal to the magnitude of the strain

580   rate tensor divided by two,

$$\left.\frac{D_M c}{Dt}\right|_{shear} = \frac{1}{2}\left(\epsilon_I - ||\mathbf{E}||\right) = -\frac{1}{2}||\mathbf{E}||.$$

When there is no shear, and only convergence, the amount of open water formation due to collisions is 10^{-7} s^{-1}, equal to the magnitude of the strain rate tensor,

$$\left.\frac{D_M c}{Dt}\right|_{conv} = \frac{1}{2}\left(\epsilon_I - ||\mathbf{E}||\right) = -\frac{1}{2}\left(|\epsilon_I| + |\epsilon_I|\right) = -||\mathbf{E}||.$$

585   In both scenarios the norm of the strain rate tensor is the same, $||\mathbf{E}|| = 10^{-7}$ s^{-1}. In the case of only shear (Fig. 4c,d), ice concentration is diminished by a factor of roughly 18%, corresponding to a 22% increase in mean ice thickness, and with no change in ice volume. In contrast, in the case of convergence only (Fig. 4a,b), ice concentration is diminished by 36%, with a corresponding 56% increase in mean ice thickness, again with no change in ice volume. Thus shear motions lead to

590   collisions and the combinations of floes with one another, but at a reduced rate when compared to convergence of ice flow, for the same strain rate tensor norm. In the case of shear only, the two initial peaks in the FSTD are smeared out over a range of floe sizes and thicknesses (Fig. 4b), with the variety of floe sizes and thicknesses increasing in number over time. Since there is twice as much open water formation in the case of convergence only, and therefore an increased number of

595   mechanical interactions, the distribution of floe sizes and thickness is smeared more rapidly, and over a larger range (Fig. 4c).

    Fig. 5 shows the response of the joint floe size and thickness distribution to a single-week experiment that simulates a seven-day period of ~~wave fracture~~ <u>ice fracture by surface waves</u>, using a wave spectrum that leads to ice breaking into a broader range of floe sizes. The experiment uses the

600   Bretschneider (Michel, 1968, p. 24) surface wave spectrum as function of period T, $S(T)\,dT$,

$$S(T)\,dT = \frac{1 H_s^2}{4\pi T_z}\left(\frac{T}{T_z}\right)^3 e^{-\frac{1}{\pi}\left(\frac{T}{T_z}\right)^4}dT,$$

where $H_s = 2$ m is the significant wave height (the mean wave height of the 1/3 highest surface waves), and $T_z = 6$ s is the mean time interval between zero-crossings of the observed wave record. We use the surface gravity wave dispersion relation $\lambda = gT^2/2\pi$ to write $S(T)\,dT$ as a wavelength

605   spectrum $S(\lambda)\,d\lambda$. The wavelength bins are spaced to correspond uniquely to floe size bins, and there is a one-to-one relationship between a wave's wavelength and the floe size of new floes formed

through fracture of existing floes by that wave. The peak wavelength of the wave spectrum is at $T \approx 7.5$ s, corresponding to $\lambda \approx 88$ m. As before, the domain width D is set to 10 kilometers. Large floes (size I) are rapidly fractured, with the fractional area corresponding to these floes is decreasing, and the distribution shifts towards smaller sizes (Fig. 5a, gray lines). After one week, the fractional area belonging to floes in the range from 75-125 m decreases from 37% to less than 1%, with mean floe size decreasing by 58% (Fig. 5b, blue line). As a consequence, the total lateral surface area rises as floes are broken and their lateral sides are exposed, increasing by 47% over the week (Fig. 5b, blue line). Over time continual fracture eliminates large floes and replaces them with smaller floes, leading to an increase in lateral surface area by 220% and a decrease in mean floe size of 73%.

4 Conclusions

~~The sea-ice floe size and thickness distribution (FSTD) may play an important role in the context of climate studies, influencing air-sea exchange, oceanic and atmospheric circulation, and sea-ice dynamics, area and thickness evolution. As ice thins, feedbacks that take place on scales smaller than the typical climate model grid scale, between the lateral sizes of floes, thermodynamic melting and freezing along floe sides and bases, ocean waves and floe collisions, may affect climate on larger scales. In addition to the FSTD being an interesting and under-explored dynamical problem, it is therefore also important to study it, develop appropriate parameterizations and represent it in global climate models.~~

We developed a model that simulates the evolution of the FSTD, using as input large-scale oceanic and atmospheric forcing fields, which may be useful as an extension to sea-ice models presently used in global climate models, in particular in regions with a continuously varying FSTD, such as the marginal ice zone. We included representations of the impact of thermodynamics (melting and freezing), mechanical interactions of rafting and ridging due to floe collisions, and of floe fracture by ocean surface waves, all processes that are active in marginal or seasonal sea-ice zones. We demonstrated the effect of these processes using model runs forced by external forcing fields including air-sea heat flux, ice flows leading to mechanical interactions, and specified surface wave field, and considered the effects of these forcing fields individually and when combined. We demonstrated the effects of mechanical interactions in the presence of both shearing and straining ice flows, separately accounting for ridging and rafting. We studied the effect of surface waves, first for idealized single-wavelength wave fields, and then accounting for a more realistic surface wave spectrum. We examined the response to melting and freezing both along existing floe bases and lateral edges, and in open water, leading to pancake ice formation.

While the present paper focuses on the development of parameterizations needed to represent the FSTD dynamics and to testing the model with individual forcing fields, we hope to next study the consequences of realistic forcing fields on the FSTD and compare model output to the few available

20

observations. Another important future direction is the model development and testing that will allow for implementation of this model into sea-ice models used in GCMs, allowing for realistic ice thermodynamics, constitutive stress-strain relationship, wave model, and ice motions driven by ocean currents and winds. At the same time, an implementation into a GCM would require making the model more efficient by replacing the high resolution we could afford to use here in floe size and thickness by a simplified approach, possibly assuming a functional form of the FSTD and simulating only its moments as is often done in atmospheric models of the particle size distribution.

The study of FSTD dynamics, and the development of a prognostic FSTD model, are made difficult by the scarcity of observations of the floe size distribution and its seasonal and long term evolution. Such observations are required to constrain uncertain parameters used in the model developed here, and help determine the dominant processes which need to be included in FSTD models to be incorporated in global climate models.

Appendix A: Comparison of rate constants in Eq. 14 to those in Thorndike et al. (1975)

Thorndike et al. (1975) employed the following parameterization of the function ψ (1), which represents the rate of change of area belonging to ice of thickness h due to mechanical interactions:

$$\psi = \left(\epsilon_I^2 + \epsilon_{II}^2\right)^{1/2} \left(\alpha_0 \delta(h) + \alpha_r w_r(h)\right), \tag{A1}$$

where $\int\limits_0^\infty w_r(h) = -1$, and the coefficients α_0 and α_c are,

$$\alpha_0 = \frac{1}{2}\left(1 + \cos(\theta)\right), \tag{A2}$$

$$\alpha_c = \frac{1}{2}\left(1 - cos(\theta)\right), \tag{A3}$$

where $\theta = \arctan(\epsilon_{II}/\epsilon_I)$. Using the trigonometric identity,

$$\cos(\arctan(\epsilon_{II}/\epsilon_I)) = \frac{\epsilon_I}{||E||},$$

with $||E|| \equiv \sqrt{\epsilon_I^2 + \epsilon_{II}^2}$, ψ may be rewritten as,

$$\psi = \frac{1}{2}||E||\left(\delta(h)\frac{||E|| + \epsilon_I}{||E||} + \frac{||E|| - \epsilon_I}{||E||}w_r\right), \tag{A4}$$

$$= \frac{1}{2}\left(\delta(h)(||E|| + \epsilon_I) + w_r(||E|| - \epsilon_I)\right), \tag{A5}$$

$$= \delta(h)\epsilon_I + \frac{1}{2}\left(||E|| - \epsilon_I\right)\left(\delta(h) + w_r\right). \tag{A6}$$

Identifying $w_r = -\int\limits_h L_c(\mathbf{r})\,dh$, and $\frac{1}{2}\left(||E|| - \epsilon_I\right) = \frac{D_M c}{Dt}$, recovers the floe-size-integrated form of (14).

References

Asplin, M. G., Galley, R., Barber, D. G., and Prinsenberg, S.: Fracture of summer perennial sea ice by ocean swell as a result of Arctic storms, J. Geophys. Res., 117, 1–12, doi:10.1029/2011JC007221, 2012.

Asplin, M. G., Scharien, R., Else, B., Howell, S., Barber, D. G., Papakyriakou, T., and Prinsenberg, S.: Implications of fractured Arctic perennial ice cover on thermodynamic and dynamic sea ice processes, J. Geophys. Res. Oceans, 119, 2327–2343, doi:10.1002/2013JC009557, 2014.

Bennetts, L. G. and Squire, V. a.: Model sensitivity analysis of scattering-induced attenuation of ice-coupled waves, Ocean Modelling, 45-46, 1–13, doi:10.1016/j.ocemod.2012.01.002, 2012.

Bennetts, L. G. and Williams, T. D.: Water wave transmission by an array of floating disks, Proc. Roy. Soc. A, 471, 1–18, doi:10.1098/rspa.2014.0698, 2015.

Birnbaum, G. and Lüpkes, C.: A new parameterization of surface drag in the marginal sea ice zone, Tellus A, 54, 107–123, doi:10.1034/j.1600-0870.2002.00243.x, 2002.

Bitz, C. M.: Numerical modeling of sea ice in the climate system, Tech. rep., University of Washington, www.atmos.uw.edu/~bitz/Bitz_chapter.pdf, 2008.

Bitz, C. M., Holland, M. M., Weaver, A. J., and Eby, M.: Simulating the ice-thickness distribution in a coupled climate model, J. Geophys. Res., 106, 2441, doi:10.1029/1999JC000113, 2001.

Bourke, R. H. and Garrett, R. P.: Sea ice thickness distribution in the Arctic Ocean, Cold Reg. Sci. Technol., 13, 259–280, doi:10.1016/0165-232X(87)90007-3, 1987.

Bouws, E., Draper, L., Shearman, E., Laing, A., Feit, D., Mass, W., Eide, L., Francis, P., Carter, D., and Battjes, J.: Guide to Wave analysis and forecasting, World Meteorological Organization, 1998, 11–12, 1998.

Cavalieri, D. J. and Parkinson, C. L.: Arctic sea ice variability and trends, 1979-2010, The Cryosphere, 6, 881–889, doi:10.5194/tc-6-881-2012, 2012.

Chevallier, M. and Salas-Mélia, D.: The role of sea ice thickness distribution in the arctic sea ice potential predictability: A diagnostic approach with a coupled GCM, J. Clim., 25, 3025–3038, doi:10.1175/JCLI-D-11-00209.1, 2012.

Collins, C. O., Rogers, W. E., Marchenko, A., and Babanin, A. V.: In situ measurements of an energetic wave event in the Arctic marginal ice zone, Geophys. Res. Lett., 42, 1863–1870, doi:10.1002/2015GL063063, 2015.

Dumont, D., Kohout, A., and Bertino, L.: A wave-based model for the marginal ice zone including a floe breaking parameterization, J. Geophys. Res., 116, C04 001, doi:10.1029/2010JC006682, 2011.

Feltham, D. L.: Granular flow in the marginal ice zone., Philosophical transactions. Series A, Mathematical, physical, and engineering sciences, 363, 1677–1700, doi:10.1098/rsta.2005.1601, 2005.

Feltham, D. L.: Sea Ice Rheology, Annual Review of Fluid Mechanics, 40, 91–112, doi:10.1146/annurev.fluid.40.111406.102151, 2008.

Girard, L., Weiss, J., Molines, J. M., Barnier, B., and Bouillon, S.: Evaluation of high-resolution sea ice models on the basis of statistical and scaling properties of Arctic sea ice drift and deformation, J. Geophys. Res., 114, C08 015, doi:10.1029/2008JC005182., 2009.

Godlovitch, D., Illner, R., and Monahan, A.: Smoluchowski coagulation models of sea ice thickness distribution dynamics, J. Geophys. Res., 116, C12 005, doi:10.1029/2011JC007125, 2011.

Harvey, L. D. D.: Testing alternative parameterizations of lateral melting and upward basal heat flux in a thermodynamic sea ice model, J. Geophys. Res., 95, 7359, doi:10.1029/JC095iC05p07359, 1990.

Henderson, G. R., Barrett, B. S., and Lafleur, D.: Arctic sea ice and the Madden–Julian Oscillation (MJO), Clim. Dynam., 43, 2185–2196, doi:10.1007/s00382-013-2043-y, 2014.

Herman, A.: Sea-ice floe-size distribution in the context of spontaneous scaling emergence in stochastic systems, Phys. Rev. E., 81, 066 123, doi:10.1103/PhysRevE.81.066123, 2010.

Herman, A.: Molecular-dynamics simulation of clustering processes in sea-ice floes, Physical Review E, pp. 1–25, 2011.

Herman, A.: Numerical modeling of force and contact networks in fragmented sea ice, Annals of Glaciology, 54, 114–120, doi:10.3189/2013AoG62A055, 2013.

Hibler, W. D.: A Dynamic Thermodynamic Sea Ice Model, J. Phys. Oceanogr., 9, 815–846, doi:10.1175/1520-0485(1979)009<0815:ADTSIM>2.0.CO;2, 1979.

Hibler III, W. D.: Modeling a variable thickness ice cover, Mon. Weath. Rev., 108, 1943–1973, 1980.

Holt, B. and Martin, S.: The effect of a storm on the 1992 summer sea ice cover of the Beaufort, Chukchi, and East Siberian Seas, J. Geophys. Res., 106, 1017, doi:10.1029/1999JC000110, 2001.

Hopkins, M. a., Tuhkuri, J., and Lensu, M.: Rafting and ridging of thin ice sheets, J. Geophys. Res., 104, 13 605, doi:10.1029/1999JC900031, 1999.

Horvat, C. and Tziperman, E.: Effects of the Sea Ice Floe Size Distribution on Polar Ocean Properties and Air-Sea Exchange, in: Abstract C11A-0341 presented at 2014 Fall Meeting, AGU, San Francisco, Calif., 15-19 Dec., p. (in prep), 2014.

Hunke, E. C., Lipscomb, W. H., Turner, A. K., Jeffery, N., and Elliot, S.: CICE: The Los Alamos Sea Ice Model Documentation and SoftwareUsers Manual Version 5.0, Tech. rep., Los Alamos Natl. Laboratory, Los Alamos, N.M., 2013.

Johannessen, J. A., Johannessen, O. M., Svendsen, E., Shuchman, R., Manley, T., Campbell, W. J., Josberger, E. G., Sandven, S., Gascard, J. C., Olaussen, T., Davidson, K., and Van Leer, J.: Mesoscale eddies in the Fram Strait marginal ice zone during the 1983 and 1984 Marginal Ice Zone Experiments, J. Geophys. Res., 92, 6754, doi:10.1029/JC092iC07p06754, 1987.

Kohout, A., Williams, M., Toyota, T., Lieser, J., and Hutchings, J.: In situ observations of wave-induced sea ice breakup, Deep Sea Research Part II: Topical Studies in Oceanography, pp. 1–6, doi:10.1016/j.dsr2.2015.06.010, 2015.

Kohout, A. L. and Meylan, M. H.: An elastic plate model for wave attenuation and ice floe breaking in the marginal ice zone, J. Geophys. Res., 113, C09 016, doi:10.1029/2007JC004434, 2008.

Lu, P., Li, Z. J., Zhang, Z. H., and Dong, X. L.: Aerial observations of floe size distribution in the marginal ice zone of summer Prydz Bay, J. Geophys. Res., 113, C02 011, doi:10.1029/2006JC003965, 2008.

McPhee, M. G.: Turbulent heat flux in the upper ocean under sea ice, J. Geophys. Res., 97, 5365, doi:10.1029/92JC00239, 1992.

Meylan, M. H., Bennetts, L. G., and a. L. Kohout: In situ measurements and analysis of ocean waves in the Antarctic marginal ice zone, Geophys. Res. Lett., 41, 1–6, doi:10.1002/2014GL060809.In, 2014.

Michel, W.: Sea Spectra Simplified, Marine Technology, 5, 17–30, 1968.

24

Niebauer, H.: Wind and melt driven circulation in a marginal sea ice edge frontal system: a numerical model, Cont. Shelf Res., 1, 49–98, doi:10.1016/0278-4343(82)90032-2, 1982.

755 Parkinson, C. L. and Washington, W. M.: A large-scale numerical model of sea ice, J. Geophys. Res., 84, 311–337, doi:10.1029/JC084iC01p00311, 1979.

Parmerter, R. R.: A model of simple rafting in sea ice, J. Geophys. Res., 80, 1948, doi:10.1029/JC080i015p01948, 1975.

Parmerter, R. R. and Coon, M. D.: Model of pressure ridge formation in sea ice, J. Geophys. Res., 77, 6565,
760 doi:10.1029/JC077i033p06565, 1972.

Perovich, D. K. and Jones, K. F.: The seasonal evolution of sea ice floe size distribution, J. Geophys. Res. Oceans, 119, 8767–8777, doi:10.1002/2014JC010136, 2014.

Renner, A. and Gerland, S.: Evidence of Arctic sea ice thinning from direct observations, Geophys. Res. Lett., 2012, 5029–5036, doi:10.1002/2014GL060369.1., 2014.

765 Rothrock, D. A. and Thorndike, A. S.: Measuring the sea ice floe size distribution, J. Geophys. Res., 89, 6477–6486, doi:10.1029/JC089iC04p06477, 1984.

Semtner, A. J.: A Model for the Thermodynamic Growth of Sea Ice in Numerical Investigations of Climate, J. Phys. Oceanogr., 6, 379–389, doi:10.1175/1520-0485(1976)006<0379:AMFTTG>2.0.CO;2, 1976.

Shen, H., Hibler, W., and Leppäranta, M.: On applying granular flow theory to a deforming broken ice field,
770 Acta Mechanica, 6Shen, H.,, 143–160, doi:10.1007/BF01182545, 1986.

Shen, H. H. and Sankaran, B.: Internal Length And Time Scales In A Simple Shear Granular Flow, Physical Review E, 70, 51 308, doi:10.1103/PhysRevE.70.051308, 2004.

Shen, H. H., Hibler, W. D., and Leppäranta, M.: The role of floe collisions in sea ice rheology, Journal of Geophysical Research, 92, 7085, doi:10.1029/JC092iC07p07085, 1987.

775 Steele, M.: Sea ice melting and floe geometry in a simple ice-ocean model, J. Geophys. Res., 97, 17 729, doi:10.1029/92JC01755, 1992.

Steer, A., Worby, A., and Heil, P.: Observed changes in sea-ice floe size distribution during early summer in the western Weddell Sea, Deep-Sea Res. II, 55, 933–942, doi:10.1016/j.dsr2.2007.12.016, 2008.

Stroeve, J. C., Serreze, M. C., Holland, M. M., Kay, J. E., Malanik, J., and Barrett, A. P.: The Arctic's rapidly
780 shrinking sea ice cover: A research synthesis, Climatic Change, 110, 1005–1027, doi:10.1007/s10584-011-0101-1, 2012.

Strong, C. and Rigor, I. G.: Arctic marginal ice zone trending wider in summer and narrower in winter, Geophys. Res. Lett., 40, 4864–4868, doi:10.1002/grl.50928, 2013.

Strong, C., Magnusdottir, G., and Stern, H.: Observed feedback between winter sea ice and the North Atlantic
785 Oscillation, J. Clim., 22, 6021–6032, doi:10.1175/2009JCLI3100.1, 2009.

Thorndike, A. S., Rothrock, D. A., Maykut, G. A., and Colony, R.: The thickness distribution of sea ice, J. Geophys. Res., 80, 4501, doi:10.1029/JC080i033p04501, 1975.

Toyota, T. and Enomoto, H.: Analysis of sea ice floes in the Sea of Okhotsk using ADEOS/AVNIR images, in: Proceedings of the 16th IAHR International Symposium on Ice, pp. 211–217, International Association of
790 Hydraulic Engineering and Research, 2002.

Toyota, T., Takatsuji, S., and Nakayama, M.: Characteristics of sea ice floe size distribution in the seasonal ice zone, Geophys. Res. Lett., 33, L02 616, doi:10.1029/2005GL024556, 2006.

Variable	Description	Section
$g(h)$	Ice thickness distribution (ITD)	1
$\mathbf{u}$	Ice velocity vector	1
ψ	Ice thickness redistribution function	1
$n(r)$	Ice floe size distribution (FSD)	1
$\mathbf{r} = (r, h)$	Floe size and thickness	1
$f(\mathbf{r})$	Joint floe size and thickness distribution (FSTD)	1
ϕ	Open water fraction	2.1
c	Ice concentration	2.1
$N(\mathbf{r})$	Floe number distribution	2.1
$C(\mathbf{r})$	Cumulative floe number distribution	2.1

Table 1. Variables appearing in several components of the FSTD model

Toyota, T., Haas, C., and Tamura, T.: Size distribution and shape properties of relatively small sea-ice floes in the Antarctic marginal ice zone in late winter, Deep-Sea Res. II, 58, 1182–1193, doi:10.1016/j.dsr2.2010.10.034, 2011.

Vavrus, S. J., Holland, M. M., Jahn, A., Bailey, D. a., and Blazey, B. a.: Twenty-first-century arctic climate change in CCSM4, J. Clim., 25, 2696–2710, doi:10.1175/JCLI-D-11-00220.1, 2012.

Washington, W. M., Semtner, A. J., Parkinson, C., and Morrison, L.: On the Development of a Seasonal Change Sea-Ice Model, J. Phys. Oceanogr., 6, 679–685, doi:10.1175/1520-0485(1976)006<0679:OTDOAS>2.0.CO;2, 1976.

Williams, T. D., Bennetts, L. G., and Squire, V. a.: Wave-ice interactions in the marginal ice zone : model sensitivity studies along a 1-D section of the Fram Strait, Ocean Model., 2012.

Williams, T. D., Bennetts, L. G., Squire, V. a., Dumont, D., and Bertino, L.: Wave–ice interactions in the marginal ice zone. Part 1: Theoretical foundations, Ocean Model., 71, 81–91, doi:10.1016/j.ocemod.2013.05.010, 2013a.

Williams, T. D., Bennetts, L. G., Squire, V. A., Dumont, D., and Bertino, L.: Wave-ice interactions in the marginal ice zone. Part 2: Numerical implementation and sensitivity studies along 1D transects of the ocean surface, Ocean Modelling, 71, 92–101, doi:10.1016/j.ocemod.2013.05.011, 2013b.

Wu, Q. and Zhang, X.: Observed evidence of an impact of the Antarctic sea ice dipole on the Antarctic oscillation, J. Clim., 24, 4508–4518, doi:10.1175/2011JCLI3965.1, 2011.

Yu, Y. and Rothrock, D. A.: Thin ice thickness from satellite thermal imagery, J. Geophys. Res., 101, 25 753, doi:10.1029/96JC02242, 1996.

Zhang, J., Lindsay, R., Schweiger, A., and Steele, M.: The impact of an intense summer cyclone on 2012 Arctic sea ice retreat, Geophys. Res. Lett., 40, 720–726, doi:10.1002/grl.50190, 2013.

Zhang, J., Schweiger, A., Steele, M., and Stern, H.: Sea ice floe size distribution in the marginal ice zone: Theory and numerical experiments, Journal of Geophysical Research: Oceans, 120, 3484—3498, doi:10.1002/2015JC010770, 2015.
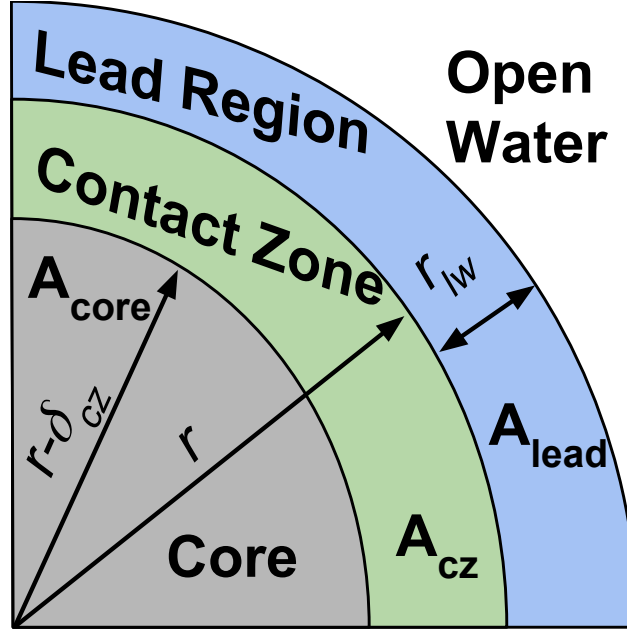
Figure 1. A section of a floe, showing the division of a floe and the surrounding sea surface for the thermo-dynamic and mechanical interaction components of the FSTD model. The floe itself, of radius r, is divided into the core which is unaffected by ridging and rafting (blue, width $r - \delta r\, r - \delta_{cz}$) and contact zone which participates in these interactions (green, width $\delta r\, \delta_{cz}$). The floe is surrounded by the lead region of width $r_p\, r_{lw}$ where net heat fluxes lead to freezing or melting of the floe itself (blue) and then by open water where cooling may lead to new pancake ice formation (white).
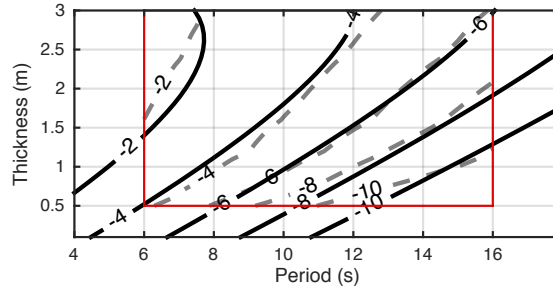
Figure 2. The natural logarithm of the attenuation coefficient α calculated by Kohout and Meylan (2008) (dash, inside the red box) and a quadratic fit to this attenuation coefficient that is used in section 2.3 (solid). Solid contours outside of the red box are extrapolated using the quadratic fit. The fit is given by $\ln \alpha(T, \bar{h}) = -0.3203 + 2.058\bar{h} - 0.9375T - 0.4269\bar{h}^2 + 0.1566\bar{h}T + 0.0006T^2$.
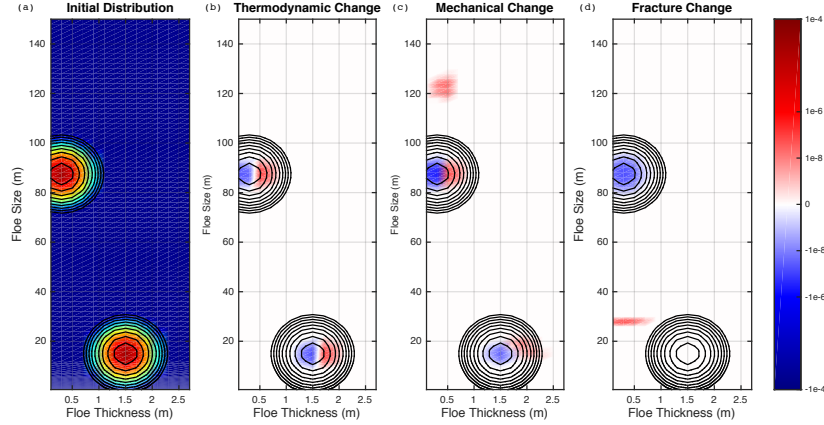
Figure 3. Response of the FSTD to idealized single-process experiments over a single time step (Section 3). (ab) Change in response to thermodynamic forcing only. (bc) Change in response to mechanical forcing only. (ed) Change in response to wave ~~fracture~~ forcing only. Solid black contours in (a-eb-d) show the initial floe size and thickness distribution, and contour intervals are powers of ten. Right color bar corresponds to the change in the FSTD in units of fractional area per timestep (1/s). Warm colors indicate an increase in fractional area, cool colors indicate a decrease in fractional area.
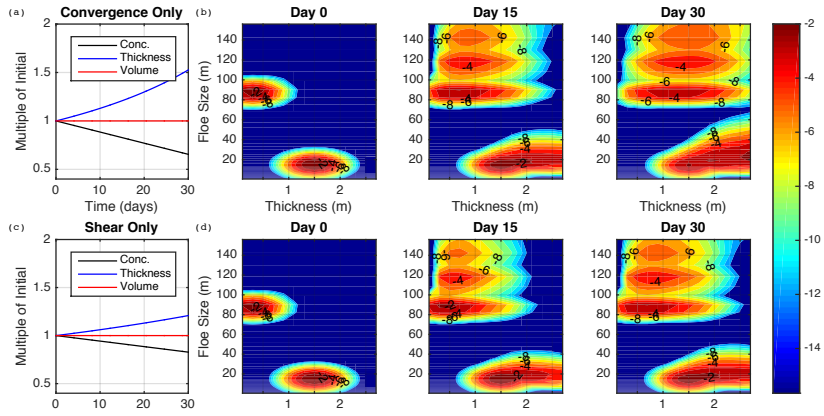
Figure 4. Results of two simulations of the floe size and thickness distribution forced with fixed ice-flow strain rates and only mechanical interactions. (a) Ice concentration, mean thickness, and ice volume for one month of fixed shear, with no convergence. Timeseries are normalized by their initial values. (b) The base 10 logarithm of the FSTD at days 0, 15, and 30 for the run with only shear. Color bar corresponds to base 10 logarithm of the FSTD, contour intervals are powers of ten. (c,d) Same as (a,b) for one week of fixed convergence with no shear.
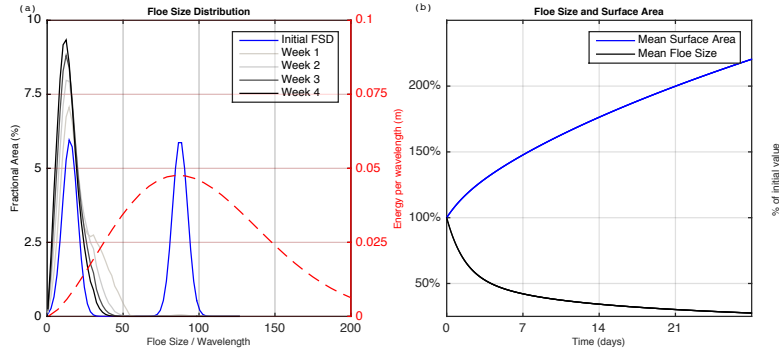
Figure 5. Results of simulations of the FSTD forced with swell fracture only. (a) The FSD before (black line, left axis) and after (grey lines line, left axis) each week of swell fracture using a Bretschneider (Michel, 1968, p. 23) wave spectrum (dashed red line, right axis). As swell fracture does not affect floe thickness, the distribution is plotted as a function of floe size only. (b) The mean floe size and total lateral ice surface area as a fraction of their initial values over the course of one week of ~~wave~~ ice fracture with the specified wave spectrum.

Variable	Description	Section
$\mathcal{L}_T$	Thermodynamic component of FSTD model	1
~~$\mathbf{G}$~~ $\mathbf{G} = (G_r, G_h)$	Ice size and thickness growth rate	2.1
~~(r_p, h_p)~~ $(r_{\min}, h_{\min})$	Size of smallest ice pancakes	2.1
r_{lw}	Width of lead region	2.1
A_{lead}	Lead area fraction	2.1
Q_{lead}	Lead area heat flux	2.1
Q_o	Open water heat flux	2.1
$\dot{A}_p$	Rate of pancake area growth	2.1
$Q_{l,l}$	Fraction of lead heat flux transmitted to floe sides	2.1
$Q_{l,b}$	Fraction of lead heat flux transmitted to floe bases	2.1

Table 2. Variables used in the representation of thermodynamical processes in the FSTD model

Variable	Description	Section
$\mathcal{L}_M$	Mechanical component of FSTD model	1
D_M/Dt	Rate of change incorporating ice collisions	2.2
L_c	Normalized fraction of concentration lost/gained by collisions	2.2
$\dot{\boldsymbol{\epsilon}}$	Ice flow strain rate tensor	2.2
$\mathbf{E}$	Vector of strain rate tensor invariants	2.2
$K(\mathbf{r}_1,\mathbf{r}_2,\mathbf{r})$	Collision kernel: two floes of size $\mathbf{r}_1$ and $\mathbf{r}_2$ forming a floe of size $\mathbf{r}$	2.2
$P_{\mathrm{coll}}(\mathbf{r}_1,\mathbf{r}_2)$	Probability of two floes of sizes $\mathbf{r}_1$ and $\mathbf{r}_2$ colliding	2.2
$\delta_{\mathrm{raft/ridge}}$	Width of contact zone for collisions rafting/ridging	2.2
A_{cz}	Area of floe contact zone	2.2
A_{core}	Area of floe core	2.2
$\gamma(h)$	Interpolation coefficient between rafting and ridging	2.2

Table 3. Variables used in the representation of mechanical interactions in the FSTD model

Variable	Description	Section
$\mathcal{L}_M$ $\mathcal{L}_W$	~~Wave~~ Ice fracture component of FSTD model	1
$\Omega(\mathbf{r},t)$	Area of floes of size $\mathbf{r}$ fractured by waves	2.3
$F(\mathbf{r},\mathbf{s})$	Floe size and thickness distribution of new floes formed by the ~~wave~~ fracture of floes of size $\mathbf{r}$ by waves	2.3
$\alpha(\lambda,h)$	Attenuation coefficient (per floe) for waves of wavelength λ encountering ice of thickness h	2.3
D	Width of computational domain onto which waves are incident	2.3
$\tau(\lambda)$	Timescale for waves of wavelength λ to cross domain	2.3
$P_f(\mathbf{r},\lambda)$	Probability that floes of size $\mathbf{r}$ will break due to waves of wavelength λ	2.3
$S(\lambda)$	Incident wave spectrum	2.3
$a(\lambda)$	Amplitude of waves of wavelength λ	2.3
ϵ_{crit}	Critical strain rate for breaking of floes	2.3
$\epsilon_{\mathrm{max}}(\lambda,h)$	Maximal strain rate experienced by a floe of thickness h due to waves of amplitude $a(\lambda)$	2.3
H_s	Significant wave height (height of 1/3 highest waves)	2.3
P_{wa}	Rayleigh distribution of surface wave heights	2.3
T_z	Zero-crossing period for wave record	3

Table 4. Variables used in the representation of ~~wave~~ the fracture of ice by surface waves in the FSTD model

A prognostic model of the sea ice floe size and thickness distribution

Christopher Horvat and Eli Tziperman

School of Engineering and Applied Sciences and Department of Earth and Planetary Sciences, Harvard University

Supplementary Materials

Contents

S1 Sensitivity tests

We examine the sensitivity of model results to perturbations in the set of parameters listed, along with sensitivity ranges, in Table S1, The perturbed parameters represent each of the model components. These tests demonstrate the robustness of the model to changes in the main model parameters, at the same time indicating the need to further constrain the relevant parameters.

S1.1 Thermodynamics

Model parameters that govern the thermodynamic model component include the pancake floe size r_{min}, pancake floe thickness h_{min}, and width of the lead region, r_{lw}. To examine the model sensitivity to changes in these parameter values, the model is initialized with zero ice concentration, with only the thermodynamic component of the model enabled. The external forcing is a net cooling heat flux $Q_{ex} = -50\mathrm{W/m}^2$, of which a proportion equal to $(1-c)Q_{ex}$, where c is the ice concentration, is applied to water (assumed to be at its freezing temperature). This cooling over water is further decomposed into an "open water" cooling of magnitude Q_o, which leads to the growth of ice pancakes, and a "lead" cooling of magnitude Q_l that leads to lateral and basal freezing, as outlined in the manuscript (Sec. 2.1). The net cooling in the region covered by ice has magnitude cQ_{ex}, and leads to only lateral and basal freezing, not to the formation of ice pancakes. To maintain a fixed grid in size and thickness space across all experiments, the pancake floe size

Parameter	Description	component	Range
r_{min}	Pancake floe size	thermo	1 m $\pm$ 0.5 m
r_{lw}	Lead region width	thermo	1 m $\pm$ 0.5 m
h_{min}	Pancake floe thickness	thermo	0.2 m $\pm$ 0.1 m
δ_{ridge}	Ridge width	mechanics	5 m $\pm$ 2.5 m
k_{ridge}	Ridging thickness mult.	mechanics	5 $\pm$ 2
v_{g}	Wave-ice group velocity	waves	$(1 \pm \frac{1}{2}) \cdot \frac{1}{2}\sqrt{g/k}$ m/s
ϵ_{crit}	Crit. failure threshold	waves	$5 \cdot 10^{-6}$ - $5 \cdot 10^{-5}$ 1/s
α	Attenuation Coefficient	waves	KM08 or BS12

Table S1: Parameters varied in sensitivity tests, with the range of values used in sensitivity tests

and thickness are specified separately from the smallest resolved floe size and thickness, which is held constant in these runs, equal to 0.5 m and 0.1 m, respectively. Each run has an evenly spaced grid of 400 floe sizes from 0.5 m to 200 m, and 14 floe thicknesses from 0.1 m to 2.7 m.

First, the pancake ice thickness, $h_{\min}$, is varied from 0.1 m to 0.3 m. Fig. S1 shows the model response in terms of the total ice volume (Fig. S1a), ice concentration (Fig. S1b) and open water cooling Q_o (Fig. S1c). All runs have the same ice volume over time, since the net cooling is fixed. When the specified pancake thickness is larger, the added area of pancakes formed by the same net cooling must decrease, as volume is conserved. Accordingly, after 15 days the ice concentration in the experiment where $h_{\min} = .3$ m is 45% of that in the experiment where $h_{\min} = .1$ m.
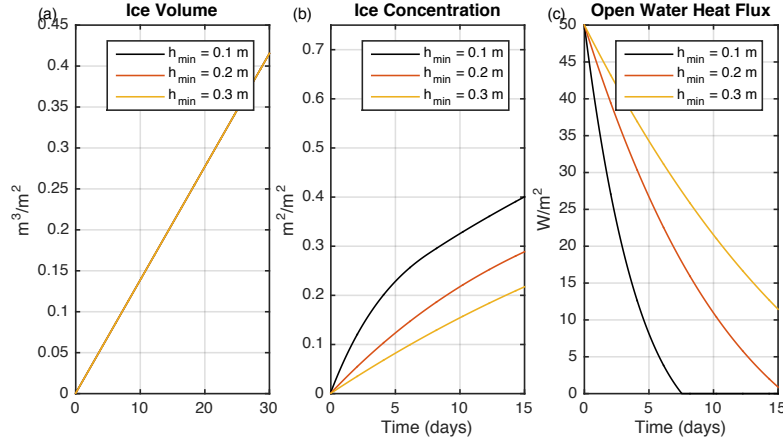
Figure S1: Sensitivity to the variation of the pancake ice thickness $h_{\min}$ from 0.1 m to 0.3 m, for an initially uncovered sea surface with a net applied cooling of 50W/m^2. (a) Ice volume, (b) ice concentration, and (c) net heat flux to the open water region for each run. Black lines correspond to default model values, $h_{\min} = 0.1$ m.

We next separately vary the lateral size of ice pancakes, $r_{\min}$, and the width of the lead region, r_{lw}, from 0.5 m to 1.5 m (Fig. S2). The ice volume is the same across both sets of runs (Fig. S2a,d), since the net cooling is fixed. First, we perturb $r_{\min}$ (Fig. S2 a-c). Since a portion of the cooling in the lead region contributes to the vertical growth of existing floes, cooling in the open water region leads to higher rates of ice concentration growth.

3

Thus, decreasing the size of the lead region leads to an increase in the rate of increase of ice concentration. Increasing the pancake floe size leads to an increase in the net open water heat flux, and therefore a more rapid increase in the ice concentration (Fig. S2b,c). After 15 days, ice concentration increases by 35% between the run in which $r_{\min} = 0.5$ m and the run in which $r_{\min} = 1.5$ m. In the second set of experiments, r_{lw} varies from 0.5 m to 1.5 m (Fig. S2d-f). Increasing the width of leads decreases the size of the open water region (Fig. S2f), leading to a slower increase in ice concentration. After 15 days, ice concentration decreases by 43% as r_{lw} increases by 200% (Fig. S2e).
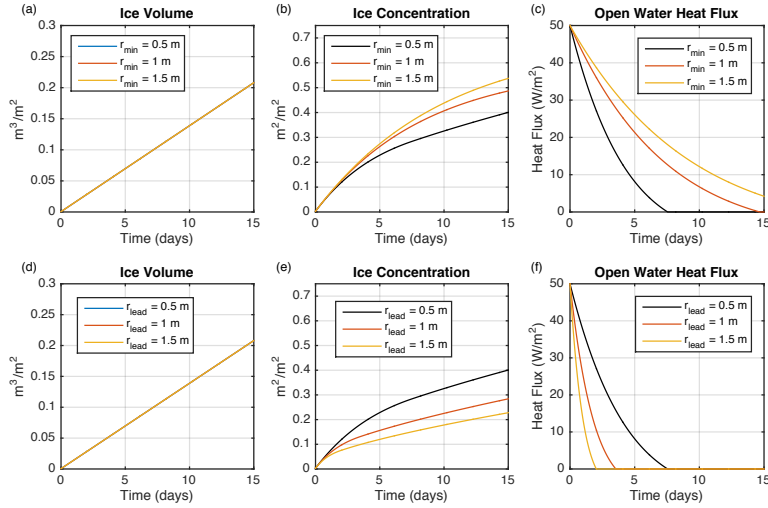
Figure S2: Sensitivity to the variation of the lead width r_{lw} and minimum floe size $r_{\min}$, for an initially uncovered sea surface with a net applied cooling of $50\mathrm{W/m^2}$. (a) Ice volume, (b) ice concentration, and (c) open water heat flux, for runs in which $r_{\min}$ is varied from 0.5 m to 1.5 m. (d-f) Same as (a-c), but when r_{lw} is varied from 0.5 m to 1.5 m. Black lines correspond to default model values, $r_{lw} = r_{\min} = 0.5$ m.

S1.2   Mechanics

This set of runs is initialized as in Sec. 3 of the manuscript, with two Gaussian peaks in the FSTD. The first peak has a mean size of 90 m and a mean

thickness of 0.25 m. The second peak has a mean size of 15 m and a mean thickness of 1.5 m, and only the mechanical component of the model is enabled. The external forcing is defined to be a set convergence of 1×10^7 1/s, applied for 30 days. These model runs are performed using the original floe size discretization outlined in the manuscript, spaced according to $r_{n+1} = \sqrt{6/5}r_n$, $r_1 = 0.5$ m, with 64 bins up to 156 m. Each run has an evenly spaced grid of 14 floe thicknesses from 0.1 m to 2.7 m.

Parameters that influence the mechanical component of the FSTD model are the widths ($\delta_{\mathrm{ridge/raft}}$) of ridges and rafts formed in floe collisions, and the thickness multiple k_{ridge}, the ratio of the thickness of a new ridge to the thickness of the smallest of two combining floes. Since we represent rafting and ridging similarly in the model, we examine only sensitivity to ridging parameters. The ridge width is varied from 3 to 7 meters, and the ridging thickness multiple is varied from 3 to 7. The response is seen in Fig. S3, note that the vertical scale is logarithmic.

The influence of changing the ridging multiple is minor, with little impact on either the FSD or ITD after 30 days (Fig. S3a,c). Changing the ridge width (Fig. S3b,d) influences the spread of smaller floes to larger sizes, and increasing the ridge width leads to more floes at smaller sizes, though the major differences are seen at sizes and thicknesses with concentration less than 1%, so the model results are largely insensitive to these parameters.

S1.3 Wave-induced fracture

This set of runs is initialized with a single Gaussian peak in the floe size distribution at 90 m size and 1 m thickness. The fracture component of the FSTD model is turned on, and all other model components are turned off. The model discretization is the same as in Sec. S1.2. The external forcing consists of a Bretschneider surface wave spectrum, with a zero-crossing period of 6 s and a significant height of 2 m, and is continuously applied for seven days at the ice edge. The model domain width is 10km.

Model parameters that influence the response of the FSTD to fracture of ice by ocean surface waves are the group velocity of waves in ice, v_{g} and the flexural strain failure threshold ϵ_{crit}. The wave group velocity is varied from 0.5 to 1.5 times the surface gravity wave group velocity. The failure threshold is varied over an order of magnitude from 5×10^{-6} 1/s to 5.5×10^{-5} 1/s. The response to the variation of these two parameters is shown in Fig. S4.

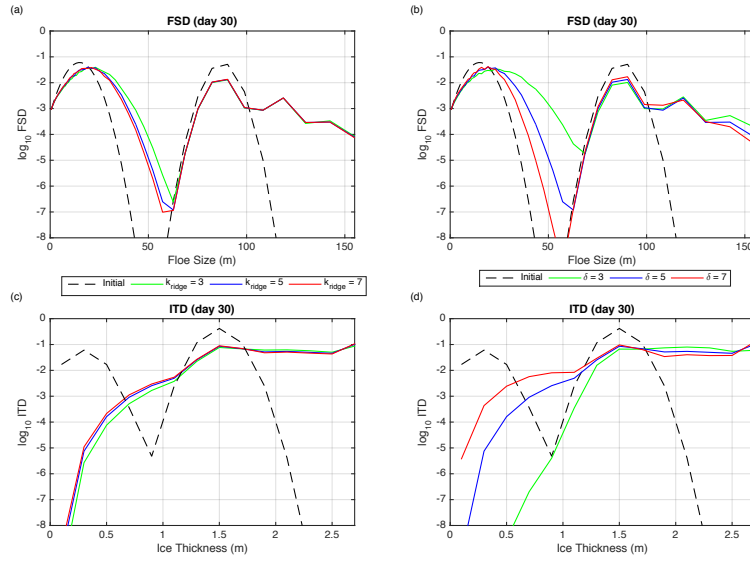The group velocity changes the fraction of the model domain affected

Figure S3: Sensitivity to the variation of ridge width and thickness multiple for the mechanical sensitivity run. (a,c) Base 10 log of the FSD (a) and ITD (c) after 30 days, when the ridging thickness multiple is changed from 3 to 7. Dashed black line is the initial condition. (b,d) Base 10 log of the FSD (b) and ITD (d) after 30 days, when the width of ridges is changed from 3 m to 7 m
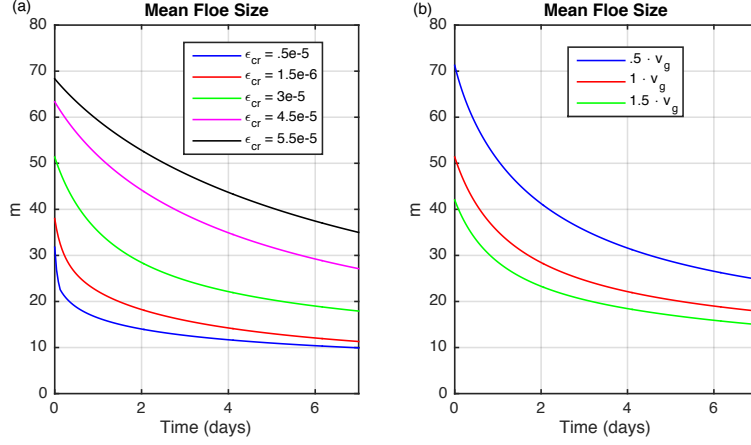
6

Figure S4: Sensitivity to the variation of parameters for runs with wave-induced fracture only, with a single Gaussian peak in the FSTD and 7 days of wave forcing. (a) Sensitivity of mean floe size to changes in ϵ_{crit}. (b) Sensitivity of mean floe size to the wave group velocity v_{g}.

by fracturing and therefore the time-scale of breaking. As the wave group velocity is increased, more fracture occurs and the mean floe size decreases (Fig. S4a). As the critical strain is increased, the amount of ice that is fractured is reduced, resulting in a higher mean floe size (Fig.'S4b).

S1.4 Attenuation model

Additionally, the parameterization of wave attenuation influences the response of the FSTD to the fracture of ice by ocean waves. We perform the same runs as in Sec. S2.2, comparing the wave attenuation model outlined in Bennetts and Squire (2012) (hereafter BS12) to the one-dimensional scattering attenuation model that is outlined and implemented in the main paper (Kohout and Meylan, 2008, herafter KM08). A comparison of the attenuation coefficient used as input in our FSTD model, as a function of wave period and ice thickness, is shown in Fig. S5 (compare with Fig. 1 in the main paper).

Fig. S6 shows how the mean floe size differs between the two simulations. The results from the run using BS12 (blue lines) have a mean floe size that is larger after one week than KM08 (red lines). The model results depend on the differences between the two parameterizations.
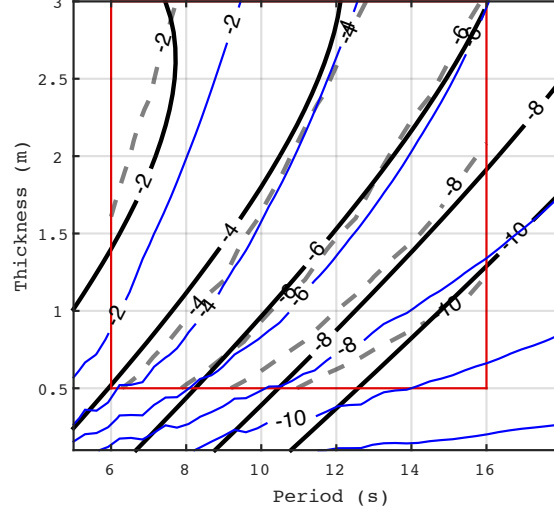
7

Figure S5: The natural logarithm of the attenuation coefficient α calculated by Kohout and Meylan (2008) (dash, inside the red box) and a quadratic fit to this attenuation coefficient that is used in section 4 of the manuscript (solid). Blue lines are the natural logarithm of the attenuation coefficient α as calculated by Bennetts and Squire (2012) and are not extrapolated. Solid contours outside of the red box are extrapolated using a quadratic fit. The fit is given by $\ln\alpha(T,\bar{h}) = -0.3203 + 2.058\bar{h} - 0.9375T - 0.4269\bar{h}^2 + 0.1566\bar{h}T + 0.0006T^2$.

S2   Numerical convergence tests

To test for numerical convergence with respect to resolution in floe-size space, we examine two single-process runs (mechanics and wave-induced fracture), which are described below. The model runs are first performed using the original resolution used in the manuscript, spaced according to $r_{n+1} = \sqrt{6/5}r_n$, $r_1 = 0.5$ m, with 64 bins up to 156 m. A second set of model runs is performed using a doubled resolution, with 63 additional floe sizes spaced evenly between gridpoints of the original grid. These tests demonstrate the robustness of the model to changes in the grid resolution.
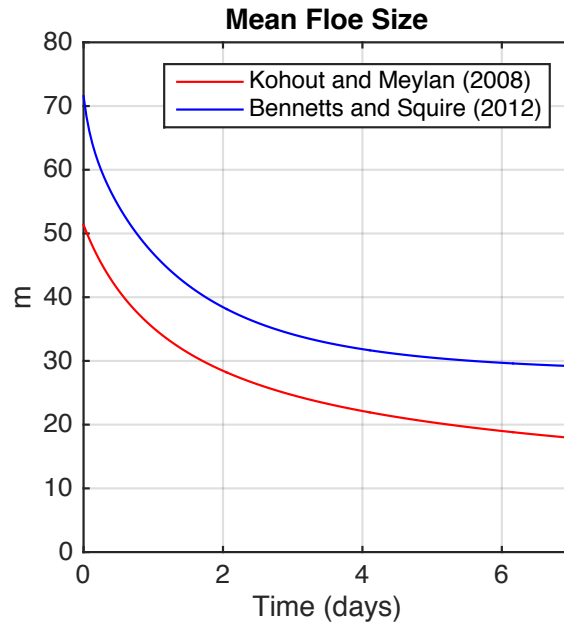
Figure S6: Comparison of the mean floe size in two week-long wave-induced fracture runs, using (red) the Kohout and Meylan (2008) or (blue) the Bennetts and Squire (2012) attenuation coefficient model. Both runs are initialized with a mean floe size of 87.5 m, the first time plotted here is the first model time step, one hour after the initialization.

S2.1   Mechanics run

The initialization is as described in section S1.2. The mechanical interaction component of the model is turned on, while all other model components are turned off, with the results of this run shown in Fig. S7. The base 10
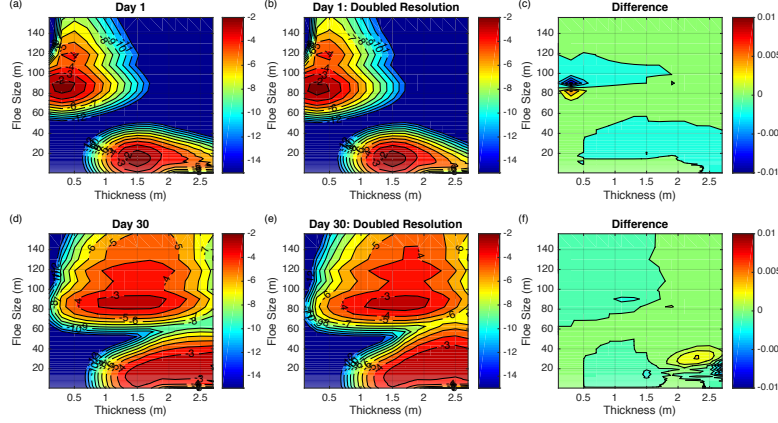

Figure S7: Base 10 logarithm of the FSTD for a regular resolution run (a,d) and doubled-resolution run (b,e) after 1 day (a-c) and 30 days (d-f). Contours are powers of ten in the distribution. (c,f) The difference (linear scale) between (a) and (b), and (d) and (e) when the doubled-resolution run is binned at the lower resolution.

logarithm of the FSTD after 1 day (Fig. S7a,d) and 30 days (Fig. S7b,e) are qualitatively similar. The difference between the two is calculated by binning the higher resolution into the lower resolution, and shows little difference between the two runs (Fig. S7c,f). The difference is nowhere larger than 1% in concentration after 30 days, so we conclude there is a limited sensitivity to resolution in these runs.

S2.2   Wave-induced fracture run

The initialization used is as described in section S1.3, and the results are seen in Fig. S8. Fig. S8a shows the base 10 logarithm of the FSD over time for the original (solid lines) and doubled (dashed lines) resolution runs, showing limited sensitivity to the shift in resolution. This is confirmed when examining the mean floe size (Fig. S8b), and additionally when examining
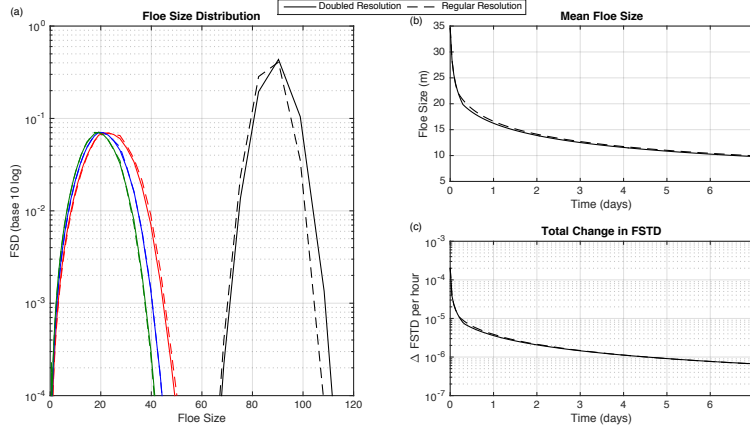
Figure S8: (a) Base 10 logarithm of the FSD for a regular resolution run (solid lines) and doubled-resolution run (dashed lines) at days 0 (black), 2 (red), 4 (blue) and 6 (green) of model runs that test convergence using wave-induced fracture alone. (b) The mean floe size over time for these runs. (c) The total fraction of the ice that is fractured, per day, for these runs.

the total area fractured per day (Fig. S8c), both of which are similar. We again conclude there is limited sensitivity to resolution in these runs.

11

References

Bennetts, L. G. and Squire, V. a. (2012). Model sensitivity analysis of scattering-induced attenuation of ice-coupled waves. *Ocean Modelling*, 45-46:1–13.

Kohout, A. L. and Meylan, M. H. (2008). An elastic plate model for wave attenuation and ice floe breaking in the marginal ice zone. *J. Geophys. Res.*, 113(9):C09016.